

Durham Research Online

Deposited in DRO:

01 June 2016

Version of attached file:

Accepted Version

Peer-review status of attached file:

Peer-reviewed

Citation for published item:

Duan, M. and Niu, Y.L. and Kong, J.J. and Sun, P. and Hu, Y. and Zhang, Y. and Chen, S. and Li, J.Y. (2016) 'Zircon U–Pb geochronology, Sr–Nd–Hf isotopic composition and geological significance of the Late-Triassic Baijiazhuang and Lvjing granitic plutons in West Qinling Orogen.', *Lithos*, 260 . pp. 443-456.

Further information on publisher's website:

<https://doi.org/10.1016/j.lithos.2016.04.015>

Publisher's copyright statement:

© 2016. This manuscript version is made available under the CC-BY-NC-ND 4.0 license
<http://creativecommons.org/licenses/by-nc-nd/4.0/>

Additional information:

Use policy

The full-text may be used and/or reproduced, and given to third parties in any format or medium, without prior permission or charge, for personal research or study, educational, or not-for-profit purposes provided that:

- a full bibliographic reference is made to the original source
- a [link](#) is made to the metadata record in DRO
- the full-text is not changed in any way

The full-text must not be sold in any format or medium without the formal permission of the copyright holders.

Please consult the [full DRO policy](#) for further details.

Accepted Manuscript

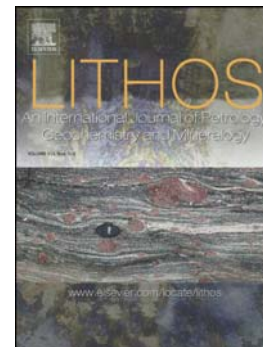
Zircon U–Pb geochronology, Sr–Nd–Hf isotopic composition and geological significance of the Late-Triassic Baijiazhuang and Lvjing granitic plutons in West Qinling Orogen

Meng Duan, Yaoling Niu, Juanjuan Kong, Pu Sun, Yan Hu, Yu Zhang, Shuo Chen, Jiyong Li

PII: S0024-4937(16)30050-0
DOI: doi: [10.1016/j.lithos.2016.04.015](https://doi.org/10.1016/j.lithos.2016.04.015)
Reference: LITHOS 3901

To appear in: *LITHOS*

Received date: 9 December 2015
Accepted date: 14 April 2016



Please cite this article as: Duan, Meng, Niu, Yaoling, Kong, Juanjuan, Sun, Pu, Hu, Yan, Zhang, Yu, Chen, Shuo, Li, Jiyong, Zircon U–Pb geochronology, Sr–Nd–Hf isotopic composition and geological significance of the Late-Triassic Baijiazhuang and Lvjing granitic plutons in West Qinling Orogen, *LITHOS* (2016), doi: [10.1016/j.lithos.2016.04.015](https://doi.org/10.1016/j.lithos.2016.04.015)

This is a PDF file of an unedited manuscript that has been accepted for publication. As a service to our customers we are providing this early version of the manuscript. The manuscript will undergo copyediting, typesetting, and review of the resulting proof before it is published in its final form. Please note that during the production process errors may be discovered which could affect the content, and all legal disclaimers that apply to the journal pertain.

Zircon U-Pb geochronology, Sr-Nd-Hf isotopic composition and geological significance of the Late-Triassic Baijiazhuang and Lvjing granitic plutons in West Qinling Orogen

Meng Duan^{1*}, Yaoling Niu^{1, 2, 3**}, Juanjuan Kong², Pu Sun², Yan Hu², Yu Zhang⁴,
Shuo Chen², Jiyong Li²

¹, School of Earth Sciences and Resources, China University of Geosciences, Beijing, 100083

², Institute of Oceanology, Chinese Academy of Sciences, Qingdao, 266071

³, Department of Earth Sciences, Durham University, Durham DH1 3LE, UK

⁴, School of Earth Sciences, Lanzhou University, Lanzhou, 730000

Correspondence :

* Miss Meng Duan (m.duan@foxmail.com)

** Professor Yaoling Niu (yaoling.niu@foxmail.com)

Abstract

The Qinling Orogen was a consequence of continental collision of the South China Craton with the North China Craton in the Triassic, and caused widespread granitoid magmatism. However, the petrogenesis of these granitoids remains controversial. In this paper, we choose the Baijiazhuang (BJZ) and Lvjing (LJ) plutons in the West Qinling Orogen for a combined study of the zircon U-Pb geochronology, whole-rock major and trace element compositions and Sr-Nd-Hf isotopic characteristics. We obtained zircon crystallization ages of ~ 216 Ma and ~ 212 Ma for the BJZ and LJ plutons, respectively. The granitoid samples from both plutons have high K_2O metaluminous to peraluminous compositions. They are enriched in large ion lithophile elements (LILEs), light rare earth elements (LREEs) and depleted in high field-strength elements (HFSEs) with significant negative Eu anomalies. The BJZ samples have initial Sr isotopic ratios of 0.7032 to 0.7078, $\epsilon_{Nd}(t)$ of -10.99 to -8.54 and $\epsilon_{Hf}(t)$ of -10.22 to -6.41. The LJ granitoids have initial Sr isotopic ratios of 0.7070 to 0.7080, $\epsilon_{Nd}(t)$ of -5.37 to -4.58 and $\epsilon_{Hf}(t)$ of -3.64 to -1.78. The enriched isotopic characteristics of the two plutons are consistent with their source being dominated by ancient continental crust. However, two BJZ samples show depleted Sr isotope compositions, which may infer possible involvement of mantle materials. Mantle-derived melt, which formed from partial melting of mantle wedge peridotite facilitated by dehydration of the subducted/subducting Mianlue ocean crust, provide the required heat for the crustal melting while also contributing to the compositions of these granitoids. That is, the two granitic plutons are magmatic

responses to the closure of the Mianlue ocean basin and the continental collision between the Yangtze and South Qinling crustal terranes.

Key words: West Qinling Orogen; Late Triassic granitoid plutons; lower crust melting; slab break-off; mantle wedge melting

1. Introduction

The Qinling Orogen is the geological boundary between the North and South China, and is located in the middle of the Central Orogenic Belt on continental China (Jiang, 1994; Zhang et al., 1998). It was formed as a result of ultimate amalgamation of the Yangtze Block with the North China Craton through two separate collisional events along the Shangdan suture in the middle Paleozoic and the Mianlue suture in the Late Triassic (Figs. 1a, b; Mattauer et al., 1985; Jiang, 1994; Ernst, et al., 1995, 2007; Zhang et al., 1998, 2004a, 2004b; Meng and Zhang, 1999, 2000; Xiao et al., 2005, 2009; Li et al., 2007; Faure et al., 2008; Dong et al., 2011). There are widespread granitoids in the western segment of the Qinling Orogen or West Qinling Orogen (Fig. 1b), which record important information on the orogenesis (Meng and Zhang, 1999; Sun et al., 2002; Zhang et al., 2007; Qin et al., 2009; Jiang et al., 2010; Dong et al., 2011, 2012a; Wang et al., 2013). Crust-mantle interaction has been widely

accepted as being responsible for the petrogenesis of these granitoids, i.e., they were derived from partial melting of the lower continental crust caused by heating from underplated mantle-derived melts (Jiang et al., 2010; Cao et al., 2011). However, controversies still exist on the origin of the mantle-derived melt (Xue et al., 1996; Sun et al., 1998, 2002; Ratschbacher et al., 2003; Li et al., 2007; Zhang et al., 2007; Qin et al., 2008a, 2008b, 2009; Jiang et al., 2010; Zhu et al., 2011; Dong et al., 2012a; Yang et al., 2014).

Decompression melting of the asthenosphere mantle, caused by the break off of the Mianlue oceanic slab, has been a popular model invoked to infer the origin of mantle-derived melt (Sun et al., 2002; Zhang et al., 2007; Zhang et al., 2009; Dong et al., 2011). The slab break-off as a trigger is possible, but whether this can induce significant asthenospheric passive upwelling and decompression melting is not as straightforward as generally perceived without question.

In this paper, we provide high quality zircon in-situ U-Pb age data, whole-rock major and trace element data and Sr-Nd-Hf isotope compositions of representative granitoid samples from the Baijiazhuang (BJZ) and Lvjing (LJ) plutons in the West Qinling Orogen to discuss the petrogenesis of these granitoids. We propose that mantle wedge melting facilitated by addition of water from the subducted Mianlue seafloor resulted in the mantle-derived melt with basaltic compositions, whose ascent and underplating caused the lower continental crust melting for the widespread granitoid magmatism. This interpretation may be simplistic, but can effectively explain the observations while also alleviating the physical difficulties associated with

the popular slab break-off model.

2. Geological background and petrology of the granitoids

2.1 Geological background

The Qinling Orogen links the Dabie-Sulu Orogen in the east and the Kunlun-Qilian Orogen in the west (Fig. 1a), and has been divided into the North and South Qinling Blocks by the Shangdan suture zone (Fig. 1b; Meng and Zhang, 1999, 2000; Zhang et al., 2007; Qin et al., 2008a; Dong et al., 2011, 2013). The South Qinling block collided with the North Qinling block in the Middle Paleozoic along the Shangdan suture (Fig. 1b). The South Qinling block was separated from the South China block during the Carboniferous to early Triassic by the paleo-Tethyan Qinling ocean (Meng and Zhang, 1999). After the closure of the paleo-Tethyan Qinling ocean, the South China block collided with the South Qinling block in the Late Triassic along the Mianlue suture, which resulted in the widespread granitic magmatism and the final amalgamation China continent (Meng and Zhang, 1999). A series of ophiolites fragments occur in the Mianlue suture zone, which have been explained to represent the remnants of the paleo-Tethyan Qinling ocean (Xu et al., 2002; Lai et al., 2008). The South Qinling block consists of Late Paleozoic medium-grade metasedimentary and metavolcanic rocks and the Triassic granitoids (Mattaue et al., 1985; Li and Sun, 1996; Qin et al., 2009). The BJZ and LJ are two plutons of these granitoids crop out in an area of $\sim 200 \text{ km}^3$ in the West Qinling Orogen. The BJZ

pluton intruded the Wujiashan Group (Fig. 1c), which is a Mesoproterozoic strata in the research area and mainly consists of banded marble, thick layered quartz marble and mica quartz schist. The LJ pluton intruded the Devonian Xihanshui Group, which consists of thick layers of limestone, calcareous sandstone, siltstone, silty shale, limestone and marlstone (Xu et al., 2006).

2.2 Petrology of the granitoids

The BJZ and LJ plutons mainly consist of medium-coarse grained biotite granite. The BJZ pluton comprises quartz (~ 25%), plagioclase (~ 30%), K-feldspar (~ 35%) and minor amphibole and biotite (~ 5%) with accessory apatite, zircon, sphene and magnetite. Compared with the BJZ pluton, the LJ pluton has similar mineral assemblages and modes except for lower modes of quartz (~ 20%) and higher modes of plagioclase (~ 35%) (Figs. 2a, b, c, and d). The LJ pluton also contains fine-grained mafic magmatic enclaves (MMEs) (Figs. 2e, f). These MMEs are 5-20 cm in size and have the same mineralogy but more mafic mineral modes (more amphibole and biotite) and higher amount of Ti-Fe oxide and apatite than the granitoid host.

3. Analytical methods

The freshest granitoid samples were chosen for geochemical analysis. Weathered surfaces, pen marks and saw marks were ground off and thoroughly cleaned. The samples were then crushed to ~ 1 cm³ size fragments and repeatedly washed with

Milli-Q water in an ultrasonic bath before being dried and ground into powders with an agate mill in a clean environment.

3.1 Major and trace element analysis

Major and trace element analysis was done at China University of Geosciences in Beijing (CUGB). Whole rock major elements were analyzed using a Leeman Prodigy Inductively Coupled Plasma Optical Emission Spectroscopy (ICP-OES) with the elemental analysis accuracy better than 5%. Analysis of USGS reference rock standards BCR-1, AGV-2 and national geological standard reference materials GSR-3 give precisions (1σ) better than 1% for most elements except for TiO_2 (~ 1.5%) and P_2O_5 (~ 2%).

Trace elements were analyzed using an Agilent-7500a ICP-MS. BCR-1 and BHVO-1 were used to monitor the analytical accuracy and precision. Analytical accuracy, as indicated by relative error between measured and recommended values is better than 5% for most elements, ranging between 10% and 13% for Cu, Sc, Nb, Er, Th, and U, and between 10% and 15% for Ta, Tm, and Gd (see Song et al., 2010b).

3.2 Sr-Nd-Hf isotopic analysis

The bulk-rock Sr-Nd-Hf isotopic compositions were analyzed at the Guangzhou Institute of Geochemistry, Chinese Academy of Sciences (GIG-CAS).

The Sr and rare earth elements (REE) were separated with cation columns, and HDEHP-coated Kef columns were used for further Nd separation. The purified Sr and

Nd were diluted in 2% HNO₃ for analysis with a Neptune ICP-MS by using a Meinhard glass nebulizer with an uptake rate of 0.1 mL/min. The Hf was separated from other elements using combination of Eichrom RE and HDEHP columns. The Hf isotopic compositions were analyzed using a Neptune MC-ICP-MS following the analytical procedure of Li et al. (2009). The measured Sr-Nd-Hf isotopic ratios were normalized to $^{86}\text{Sr}/^{88}\text{Sr} = 0.1194$, $^{146}\text{Nd}/^{144}\text{Nd} = 0.7219$, and $^{179}\text{Hf}/^{177}\text{Hf} = 0.7325$, respectively. See Li et al. (2006) for details of analytical procedures.

3.3 Zircon LA-ICP-MS U-Pb dating

Two granitoid samples from the Baijiazhuang (BJZ12-04) and Lvjing (DHG12-01) plutons were chosen for zircon U-Pb dating at CUGB. The instrument couples a quadrupole ICP-MS (Agilent 7500a) and an UP-193 Solid-State laser (193 nm, New Wave Research Inc.) with an automated positioning system (Song et al., 2010a). During the analysis, laser spot size was set at ~36 μm with laser energy density at 8.5 J/cm² and repetition rate at 10 Hz. The specific procedure of laser sampling is 5-s pre-ablation, 20-s flushing sample-chamber and 40-s data collection. The high-purity helium gas stream was used with flux of 0.8 L/min and the ablated material was carried into the ICP-MS. In order to ensure energy stability, the whole laser path was fluxed with N₂ (15 L/min) and Ar (1.15 L/min). The counting time for U, Th, ^{204}Pb , ^{206}Pb , ^{207}Pb and ^{208}Pb is 20 ms, and is 15 ms for other elements (Song et al., 2010a). Zircon 91500 is used as external standard to correct for U-Pb isotope fractionation effects (Wiedenbeck et al., 1995). The isotopic ratios and element

concentrations of zircon were calculated with GLITTER 4.4. The concordia ages and diagrams were made using Isoplot/Ex (3.0) (Ludwig, 2003).

4. Results

4.1 Zircon LA-ICP-MS U-Pb ages

Representative CL images of analyzed zircons are shown in Appendix 1 and the U-Pb ages are given in Appendix 2.

Zircons from sample BJZ12-04 (from the BJZ pluton) are subhedral to euhedral. They have varying sizes of 100 to 300 μm , length/width ratios of 2:1 to 6:1 and clear oscillatory zoning in the CL images (Appendix 1), suggesting a magmatic origin (Pupin, 1980; Corfu et al., 2003). Twenty-five zircons show varying U (374-3728 ppm), Th (93-1436 ppm) and Th/U (0.1-1.1; mostly less than 1). Nineteen analyses of 25 zircons give a weighted average $^{206}\text{Pb}/^{238}\text{U}$ age of 216 ± 1.8 Ma (2σ ; MSWD = 1.5), which is interpreted as the crystallization age of the BJZ pluton (Fig. 3). The other six analyses with discordance >10% (Appendix 2) were rejected to plot into the Concordance diagram.

Zircons from sample DHG12-01 (from the LJ pluton) are more euhedral than those from the BJZ pluton. They are ~ 100 to 300 μm in size and have varying length/width ratio of 1:1-3:1 (Appendix 1). They show clear oscillatory zoning in the CL images, which is also indicative of a magmatic origin (Corfu et al., 2003). Thirty zircons show varying U (143-1412 ppm), Th (81-433 ppm) and Th/U (0.25-0.96). The

ages of LJ samples plot in two groups with ages of ~ 225 Ma and ~ 212 Ma, respectively, with an average age of 217.5 ± 2.5 Ma (Fig. 3b). The bimodal ages may represent two batches of magmatic events (e.g., a composite pluton). We interpret the ~ 212 Ma as representing the final crystallization age of the LJ pluton, and zircons of ~ 225 Ma may represent “xenocrysts” from prior batch of magma.

4.2 Major and trace elements

Appendix 3 gives the analytical data.

The samples from the BJZ pluton have high SiO_2 (72.58-76.60 wt.%), Al_2O_3 (12.07-14.91 wt.%), total alkalis ($\text{Na}_2\text{O} + \text{K}_2\text{O} = 8.29$ -9.01 wt.%) and $\text{K}_2\text{O}/\text{Na}_2\text{O}$ (1.30-1.72), and low TiO_2 (0.12-0.18 wt.%), MgO (0.16-0.33 wt.%), $\text{Fe}_2\text{O}_{3\text{T}}$ (0.88-1.31 wt.%) and CaO (0.62-0.98 wt.%) (Appendix 3). They plot in the granite field in the TAS diagram (Fig. 4a). The aluminum saturation index ($\text{ASI} = \text{molar } \text{Al}_2\text{O}_3 / (\text{Na}_2\text{O} + \text{K}_2\text{O} + \text{CaO})$) varies from weakly metaluminous to peraluminous (Fig. 4b).

Samples from the LJ pluton, on the other hand, have relatively lower SiO_2 (69.52-71.95 wt.%), total alkalis (7.56-8.74 wt.%), $\text{K}_2\text{O}/\text{Na}_2\text{O}$ (1.36-1.55) and relatively higher TiO_2 (0.25-0.37 wt.%), MgO (0.64-0.91 wt.%), $\text{Fe}_2\text{O}_{3\text{T}}$ (1.96-2.82 wt.%) and CaO (1.43-1.99 wt.%) (Fig.5). They plot in the granite (Fig. 4a) and peraluminous fields (Fig. 4b) with $\text{ASI} > 1$ (0.99-1.12). Compared with the granitoid host, the MMEs from the LJ pluton have lower SiO_2 , total alkalis and higher TiO_2 , Al_2O_3 , CaO , MgO and $\text{Fe}_2\text{O}_{3\text{T}}$, with a small $\text{Mg}^\#$ ($= \text{molar } 100 * \text{Mg}^{2+} / [\text{Fe}^{2+} + \text{Mg}^{2+}]$)

variation (52.7-53.4) (Appendix 3; Fig. 5). They plot in the monzonite and granodiorite fields (Fig. 4a) and in the metaluminous field (Fig. 4b).

In chondrite-normalized REE diagrams (Figs. 6a, c), granitoid samples from the BJZ and LJ plutons show LREE enrichment and HREE depletion with large $(La/Yb)_N$ variations of 11.19-30.75 and 13.24-22.87, respectively. All the samples show flat HREE patterns with $(Dy/Yb)_N \sim 1.09$ -1.65 for the BJZ pluton and ~ 1.29 -1.51 for the LJ pluton, suggesting the absence of garnet in their petrogenesis. Negative Eu anomalies exist in all the granitoid samples. However, samples from the BJZ pluton have greater negative Eu anomalies ($Eu/Eu^* = 0.23$ -0.43; $Eu/Eu^* = 2Eu_N/(Sm_N + Gd_N)$) than those from the LJ pluton ($Eu/Eu^* = 0.47$ -0.78). The MMEs show similar REE patterns with DHG12-06 and DHG12-09 showing moderate and weak negative Eu anomalies, respectively.

In the primitive mantle normalized multi-element diagrams (Figs. 6b, d), samples from both plutons show spikes of large ion lithophile elements (LILE; e.g., Th, U, K, Pb) and troughs of high field strength elements (HFSE; e.g., Nb, Ta, Ti, P), resembling the bulk continental crust (BCC; Rudnick and Gao, 2003). The two MMEs from the LJ pluton show similar trace element patterns with the host granites but with weak or absence of troughs of P and Ti, which is consistent with the higher modes of apatite and Fe-Ti oxides in the MMEs.

4.3 Bulk-rock Sr-Nd-Hf isotopes

Isotopic compositions of all the analyzed samples are given in Appendix 4 and

shown in Figs. 7a, b.

The samples from the BJZ pluton have initial Sr isotopic ratios of 0.7033-0.7068, $\epsilon_{\text{Nd}}(t)$ of -10.95 to -8.50 and $\epsilon_{\text{Hf}}(t)$ of -10.14 to -6.33. Whole-rock Nd isotope model ages (T_{DM}) range from 1.6 to 2.2 Ga. Single stage Hf model ages (T_{DM1}) are from 1.3 to 1.7 Ga and two stage Hf model ages (T_{DM2}) are from 1.7 to 1.9 Ga.

The granitoids from the LJ pluton have relatively uniform Sr ($(^{87}\text{Sr}/^{86}\text{Sr})_i \sim 0.7070$ -0.7079), Nd ($\epsilon_{\text{Nd}}(t) \sim -5.35$ to -4.56) and Hf ($\epsilon_{\text{Hf}}(t) \sim -3.59$ to -1.74) isotopes. The whole-rock Nd isotopic model ages (T_{DM}) are essentially the same of ~ 1.3 -1.4 Ga, so are the single stage Hf model ages ($T_{\text{DM1}} \sim 1.0$ -1.1 Ga) and two stage Hf model ages ($T_{\text{DM2}} \sim 1.5$ -1.6 Ga).

The two MMEs from the LJ pluton have similar Nd ($\epsilon_{\text{Nd}}(t) \sim -4.90$ to -3.52) and Hf ($\epsilon_{\text{Hf}}(t) \sim -1.34$ to +2.41) isotopes, but rather different Sr isotopic compositions with DHG12-06 being much more radiogenic $(^{87}\text{Sr}/^{86}\text{Sr})_i$ of 0.7161 (Fig. 7a), which may result from addition of upper crust materials during magma evolution or during the production of mantle-derived melt (see below).

5. Discussion

5.1 Origin of the LJ MMEs

The origin of the MMEs in granitoids has long been debated. One popular explanation is magma mixing between mafic and felsic magmas (Vernon, 1984; Baxter and Feely, 2002; Zhang et al., 2007; Qin et al., 2008a, 2009; Dong et al., 2011).

However, this mechanism cannot explain the widely observed rather similar/overlapping isotopic compositions between the MMEs and the granitoid host simply because it is physically unlikely that isotopic are homogenized while major and trace elements are not during magma mixing (Niu et al., 2013). Another interpretation is that MMEs represent cumulates from more primitive andesitic melt of the same magmatic system (Barbarin, 2005; Niu et al., 2013; Huang et al., 2014; Chen et al., 2015).

The MMEs in the LJ pluton have no chilled margins at contacts with the host granitoids. They are elliptical and have similar mineral assemblages as the granitoids but with greater mafic (e.g., amphibole) mineral modes, indicating that the MMEs in the LJ pluton were not formed by magma mixing (Niu et al., 2013; Chen et al., 2015). Because of the first order correlated variations in major elements of MMEs and host granitoids (Fig. 5), and similar REE and trace element patterns (Fig. 6), we consider the MMEs are consistent with being of cumulate origin from an earlier batch of andesitic melt (also see Chen et al., 2015).

The high $(^{87}\text{Sr}/^{86}\text{Sr})_i$ of MME DHG12-06 likely represents cumulate from a parental magma with high $(^{87}\text{Sr}/^{86}\text{Sr})_i$, which may result from greater extent of crustal assimilation although we cannot rule out the possibility of terrigenous sediment contribution to mantle wedge melting source region for mantle-derived melt (see below). If the parental magmas represent early batches of melt intruding the crustal magma chamber, it would have been assimilated more of the crust materials with evolved Sr isotopic compositions inherited in the cumulated MMEs. These MMEs can

be captured by the granitic melt later intruded in the magma chamber, and then fractionated from the granitic melt together with the minerals crystallized. Generally, MME DHG12-06 and the granites are accumulated from different batches of magmas with different isotopic compositions in a periodically replenished magma chamber.

5.2 Petrogenesis of the BJZ and LJ plutons

5.2.1 Crystallization evolution

As mentioned above, the granitoids from the BJZ pluton are relatively more felsic than those from the LJ pluton (Fig. 5), which are consistent with their crystallizing from a more evolved parental magma than the LJ samples. Compared with the samples from the LJ pluton, those from the BJZ pluton exhibit lower Sr content and more significant negative Sr anomalies with $Sr/Sr^* (= 2Sr_N / [Pr_N + Nd_N])$ 0.18-0.35 (Figs. 6, 8), corresponding to greater negative Eu anomalies (Fig. 8), which is consistent with the BJZ samples being more evolved with a greater extent of plagioclase fractionation. One MME (DHG12-06) shows higher Sr/Sr^* and Eu/Eu^* than the granitoid host, and the other MME (DHG12-09) has intermediate Sr/Sr^* and higher Eu/Eu^* (Fig. 8), which are consistent with their cumulating origin in the early stage of the magma evolution (see above).

5.2.2 Source of the granitoids

The granite samples are enriched in LILEs (Th, U, K, Pb) and LREEs, and

depleted in HFSEs (Nb, Ta, Ti, P) (Fig. 6), similar to the continental crust. In the $(^{87}\text{Sr}/^{86}\text{Sr})_i$ vs. $\epsilon_{\text{Nd}}(t)$ diagram (Fig. 7a), isotopic compositions of other Triassic granitic plutons in the Qinling Orogen are plotted for comparison (e.g. the Guangtoushan-Liuba, Mishuling and Wenquan plutons; Zhang et al., 2006; Qin et al., 2009; Cao et al., 2011). The granitoid samples of the BJZ and LJ plutons, similar to other granitoids in the Qinling Orogen, have evolved isotopic compositions with $(^{87}\text{Sr}/^{86}\text{Sr})_i$ of most samples ranging from 0.704 to 0.710, negative $\epsilon_{\text{Nd}}(t)$ (-10.95 to -8.50) and $\epsilon_{\text{Hf}}(t)$ (-10.14 to -6.33) (Fig. 7), which is consistent with these granitoids being derived from lower continental crust (Zhang et al., 2007; Qin et al., 2009; Wang et al., 2013). The whole-rock Nd isotopic model ages (T_{DM} ; 1.6-2.2 Ga and 1.3-1.4 Ga, respectively) and single stage Hf model ages (T_{DM1} ; 1.3-1.7 Ga and 1.0-1.1 Ga, respectively) of BJZ and LJ granites also support a source composed of ancient lower continental crust (Zhang et al., 2007; Qin et al., 2009). The two stage Hf model ages (T_{DM2}) of BJZ and LJ granites are 1.7-1.9 Ga and 1.5-1.6 Ga, respectively, suggesting the granites deriving from reworking of Late Palaeoproterozoic to Early Mesoproterozoic crust. However, several samples which have lower $(^{87}\text{Sr}/^{86}\text{Sr})_i$ (e.g. BJZ12-04, LZG12-07) or higher $\epsilon_{\text{Nd}}(t)$ (> -10) (Fig. 7a) indicate that the lower continental crust is not their only source component and materials with depleted isotopic compositions must have been involved in the melting process. Such depleted materials are most probably mantle-derived (Sun et al., 2002; Qin et al., 2008b).

5.2.3 Origin of mantle-derived melt

Granitoid magmatism in the continental collision belts is explained to result from lithospheric delamination (Bird, 1979) or break-off of the oceanic slab from the buoyant continental lithosphere (Davies and von Blanckenburg, 1995). In Bird (1979), the delamination of continental lithospheric mantle is invoked to provide a conduit enabling the asthenosphere to arise to the base of the continental crust and induce granitoid magmatism. However, the delamination of the continental lithospheric mantle is physically difficult because the lithospheric mantle with high $Mg^{\#}$ and low Al_2O_3 content has lower density relative to the underlying asthenosphere due to the history of high extent melt extraction (Niu et al., 2003; Niu and O'Hara, 2008).

Asthenosphere upwelling induced by the oceanic slab break-off is more widely used in interpreting the granitoid magmatism in the continental collision belt (Davis and von Blanckenburg, 1995; Sun et al., 2002; Zhang et al., 2007; Zhang et al., 2009; Dong et al., 2011). However, this model also has problems. Firstly, slab break-off cannot produce stationary lithospheric window adequate for continued asthenospheric upwelling and decompression melting as it would take place beneath ocean ridges (Klein and Langmuir, 1987; McKenzie and Bickle, 1988; Niu and Batiza, 1991; Niu and O'Hara, 2008). Therefore, the amount of mantle-derived melt produced by slab breakoff must be limited in volume and cannot be an effective cause for significant crustal melting required by the widespread and voluminous granitoid magmatism in the West Qinling orogenic belt (Zhang et al., 2007; Fig. 1b). Furthermore, the absence of high pressure metamorphic rocks in the Qinling orogen indicates that the slab break-off, if there was any, happened at a shallow depth, which has been explained to

enable the upwelling asthenosphere to impinge on the base of lower continental crust (Sun et al., 2002; Qin et al., 2008). However, as we mentioned above, asthenosphere cannot simply heat the crust to melt without removing the buoyant continental lithospheric mantle.

Here we propose a much simpler model that is consistent with the observations and basic petrological concepts. That is, ascent and underplating of basaltic melt of mantle wedge origin can cause lower continental crust melting to account for the granitoids. When the Mianlue oceanic slab subducted beneath the South Qinling Block, dehydration of the ocean crust can effectively lower the solidus of mantle wedge peridotite to melt for the basaltic melt (e.g. Pearce and Peate, 1996). Extraction, ascent and underplating of such mantle wedge-derived basaltic melt can induce the lower continental crustal melting to produce magmas parental to the BJZ and LJ granitoids (Fig. 9). Such mantle-derived melt, also contributes materials to the granitoid magmatism, i.e., there exists mixing between the mantle-derived isotopically depleted melt and isotopically enriched felsic melt from the lower continental crust, which is consistent with variable isotope compositions (Fig. 7).

Furthermore, terrigenous sediment, which may transports as melt or fluid from the subducted ocean slab to the overlying mantle wedge (Nichols et al., 1994; Johnson and Plank, 2000; Elliott, 2003) and give the mantle-derived melt isotopically more enriched character, has long been recognized to contribute to the source of the island arc basalts (IAB) (Morris et al., 1990; Vroon et al., 1993; Davidson, 1996; Elliott, 2003). Such mantle-derived melt, when mixing with a high proportion with the melt

from the lower continental crust, can crystalize mineral assemblages with enriched isotopic characters (e.g. MME DHG12-06; Fig. 7a).

5.2.4 Implications for the division of syn-collisional or post-collisional granitoids

Many studies refer the formation stage of the granitic plutons as syn-collisional or post-collisional using various geochemical discrimination diagrams (Pearce et al., 1984; Harris et al., 1986; Maniar et al., 1989; Barbarin et al., 1999; Zhang et al., 2007; Qin et al., 2008a; Dong et al., 2011, 2012a; Zhu et al., 2011). However, collision by itself does not generate sufficient heat, creates no scenario for decompression nor source of water addition, and thus cannot produce large volumes of granitic magmas (Niu, 2005). The precise timing to distinguish syn-collisional and post-collisional processes is in itself vague and cannot be constrained. The ages of Triassic granites in the Qinling Orogen have been popularly invoked as representing the time of oceanic slab break-off after the collision, with the assumption that slab break-off induced the upwelling of asthenospheric mantle and thus the formation of widespread Triassic granitic plutons in the Qinling Orogen (Sun et al., 2002; Qin et al., 2008b). However, such an assumption on the petrogenesis of Triassic granites in the Qinling Orogen is far from robust as discussed above. Thus, even though there may be some genetic relationship between the collision and the granitoid magmatism, caution is needed when applying the geochemical or chronological data to “constrain” the nature and timing of the events that actually cannot yet be constrained, for which genuine efforts are needed in future studies.

6. Conclusion

- (1) Zircon U-Pb dating give ages of ~216 and 212 Ma for the BJZ and LJ plutons, respectively.
- (2) The MMEs in the LJ pluton represent cumulate from the more primitive andesitic melt in the early stage of the magmatic evolution.
- (3) The enriched Sr-Nd-Hf isotope compositions suggest that their main source is the ancient lower continental crust. However, components from depleted mantle wedge and upper crust materials must have been involved in the formation process of the granitic magmas.
- (4) We emphasize that seafloor slab dehydration induced mantle wedge melting remains the primary mechanism for mantle-derived basaltic melts, whose underplating and intrusion of the crust can cause continental crustal melting. The popular slab break-off model cannot produce volumetrically significant mantle-derived melt and also cannot fix the problem of asthenospheric upwelling without removing the buoyant continental lithospheric mantle to account for the widespread granitic plutons in the Qinling Orogen.

Acknowledgements

We thank Prof. Li Su (the Geologic Lab Center, China University of Geosciences, Beijing) for the help with major and trace elements analysis and zircon LA-ICP-MS

U-Pb dating. We also thank Prof. Jinlong Ma (the Guangzhou Institute of Geochemistry, Chinese Academy of Sciences) for the Sr-Nd-Hf isotopic analysis. This study is supported by the National Natural Science Foundation of China (91014003, 41130314).

References

- Barbarin, B., 1999. A review of the relationships between granitoid types, their origins and their geodynamic environments. *Lithos* 46, 605-626.
- Barbarin, B., 2005. Mafic magmatic enclaves and mafic rocks associated with some granitoids of the central Sierra Nevada batholith, California: nature, origin, and relations with the hosts. *Lithos* 80, 155-177.
- Baxter, S., Feely, M., 2002. Magma mixing and mingling textures in granitoids: examples from the Galway Granite, Connemara, Ireland. *Mineralogy and Petrology* 76, 63-74.
- Bird, P., 1979. Continental delamination and the Colorado Plateau. *J. geophys. Res* 84, 7561-7571.
- Cao, X.F., Lü, X.B., Yao, S.Z., Mei, W., Zou, X.Y., Chen, C., Liu, S.T., Zhang, P., Su, Y.Y., Zhang, B., 2011. LA-ICP-MS U-Pb zircon geochronology, geochemistry and kinetics of the Wenquan ore-bearing granites from West Qinling, China. *Ore Geology Reviews* 43, 120-131.
- Chen, S., Niu, Y.L., Sun, W.L., Zhang, Y., Li, J.Y., Guo, P.Y., Sun, P., 2015. On the origin of mafic magmatic enclaves (MMEs) in syn-collisional granitoids: evidence from the Baojishan pluton in the North Qilian Orogen, China. *Mineralogy and Petrology*, 1-20.
- Corfu, F., Hanchar, J.M., Hoskin, P.W., Kinny, P., 2003, Atlas of zircon textures. *Reviews in*

- Mineralogy and Geochemistry 53, 469-500.
- Davies, J.H., von Blanckenburg, F., 1995. Slab breakoff: a model of lithosphere detachment and its test in the magmatism and deformation of collisional orogens. *Earth and Planetary Science Letters* 129, 85-102.
- Davidson, J. P. (1996). Deciphering mantle and crustal signatures in subduction zone magmatism. *Subduction top to bottom*, 251-262.
- Dong, Y.P., Liu, X.M., Neubauer, F., Zhang, G.W., Ni, T., Zhang, Y.G., Zhang, X.N., Li, W., 2013. Timing of Paleozoic amalgamation between the North China and South China Blocks: evidence from detrital zircon U-Pb ages. *Tectonophysics* 586, 173-191.
- Dong, Y.P., Liu, X.M., Santosh, M., Chen, Q., Zhang, X.N., Li, W., He, D.F., Zhang, G.W., 2012a. Neoproterozoic accretionary tectonics along the northwestern margin of the Yangtze Block, China: constraints from zircon U-Pb geochronology and geochemistry. *Precambrian Research* 196, 247-274.
- Dong, Y.P., Liu, X.M., Zhang, G.W., Chen, Q., Zhang, X.N., Li, W., Chen, Y., 2012b. Triassic diorites and granitoids in the Foping area: Constraints on the conversion from subduction to collision in the Qinling orogen, China. *Journal of Asian Earth Sciences* 47, 123-142.
- Dong, Y.P., Zhang, G.W., Neubauer, F., Liu, X.M., Genser, J., Hauzenberger, C., 2011. Tectonic evolution of the Qinling orogen, China: review and synthesis. *Journal of Asian Earth Sciences* 41, 213-237.
- Ernst, W.G., Liou, J.G., 1995. Contrasting plate-tectonic styles of the Qinling-Dabie-Sulu and Franciscan metamorphic belts. *Geology* 23, 353-356.
- Ernst, W.G., Tsujimori, T., Zhang, R., Liou, J., 2007. Permo-Triassic collision, subduction-zone

- metamorphism, and tectonic exhumation along the East Asian continental margin. *Annu. Rev. Earth Planet. Sci.* 35, 73-110.
- Elliott, T. (2003). Tracers of the slab. *Inside the subduction factory*, 23-45.
- Faure, M., Lin, W., Monié, P., Meffre, S., 2008. Palaeozoic collision between the North and South China blocks, Triassic intracontinental tectonics, and the problem of the ultrahigh-pressure metamorphism. *Comptes Rendus Geoscience* 340, 139-150.
- Geological Map 1/250,000 (2007) (Chinese Geological Regional Survey and Geological Investigation Institute of Gansu Province).
- Harris, N.B., Pearce, J.A., Tindle, A.G., 1986. Geochemical characteristics of collision-zone magmatism. *Geological Society, London, Special Publications* 19, 67-81.
- Huang, H., Niu, Y.L., Nowell, G., Zhao, Z.D., Yu, X.H., Zhu, D.C., Mo, X.X., Ding, S., 2014. Geochemical constraints on the petrogenesis of granitoids in the East Kunlun Orogenic belt, northern Tibetan Plateau: Implications for continental crust growth through syn-collisional felsic magmatism. *Chemical Geology* 370, 1-18.
- Jaques, A., Green, D., 1980. Anhydrous melting of peridotite at 0–15 kb pressure and the genesis of tholeiitic basalts. *Contributions to mineralogy and petrology* 73, 287-310.
- Jiang, C.F., 1994. On Major Tectonic Characteristics of the Central Orogenic Belt, *Dixue Yanjiu*, 2 (in Chinese).
- Jiang, Y.H., Jin, G.D., Liao, S.Y., Zhou, Q., Zhao, P., 2010. Geochemical and Sr–Nd–Hf isotopic constraints on the origin of Late Triassic granitoids from the Qinling orogen, central China: implications for a continental arc to continent-continent collision. *Lithos* 117, 183-197.
- Johnson, M. C. & Plank, T. (2000). Dehydration and melting experiments constrain the fate of sub

- ducted sediments. *Geochemistry, Geophysics, Geosystems* 1.
- Klein, E.M., Langmuir, C.H., 1987. Global correlations of ocean ridge basalt chemistry with axial depth and crustal thickness. *J. geophys. Res* 92, 8089-8115.
- Lai, S.C., Qin, J.F., Chen, L., Grapes, R., 2008. Geochemistry of ophiolites from the Mian-Lue Suture Zone: implications for the tectonic evolution of the Qinling Orogen, Central China. *International Geology Review* 50, 650-664.
- Li, S.Z., Kusky, T.M., Wang, L., Zhang, G.W., Lai, S.C., Liu, X.C., Dong, S.W., Zhao, G.C., 2007. Collision leading to multiple-stage large-scale extrusion in the Qinling orogen: insights from the Mianlue suture. *Gondwana Research* 12, 121-143.
- Li, X.H., Li, W.X., Li, Z.X., Lo, C.H., Wang, J., Ye, M.F., Yang, Y.H., 2009. Amalgamation between the Yangtze and Cathaysia Blocks in South China: constraints from SHRIMP U–Pb zircon ages, geochemistry and Nd–Hf isotopes of the Shuangxiwu volcanic rocks. *Precambrian Research* 174, 117-128.
- Li, X.H., Li, Z.X., Li, W.X., Wang, Y.J., 2006. Initiation of the Indosinian Orogeny in South China: evidence for a Permian magmatic arc on Hainan Island. *The Journal of geology* 114, 341-353.
- Ludwig, K.R., 2003. User's manual for Isoplot 3.00: a geochronological toolkit for Microsoft Excel. Kenneth R. Ludwig.
- Maniar, P.D., Piccoli, P.M., 1989. Tectonic discrimination of granitoids. *Geological society of America bulletin* 101, 635-643.
- Mattauer, M., Matte, P., Malavieille, J., Tapponnier, P., Maluski, H., Qin, X.Z., Lun, L.Y., Qin, T.Y., 1985. Tectonics of the Qinling belt: build-up and evolution of eastern Asia. *Nature* 317, 496-500.

- Meng, Q.R., Zhang, G.W., 1999. Timing of collision of the North and South China blocks: controversy and reconciliation. *Geology* 27, 123-126.
- Meng, Q.R., Zhang, G.W., 2000. Geologic framework and tectonic evolution of the Qinling orogen, central China. *Tectonophysics* 323, 183-196.
- Mo, X.X., Niu, Y.L., Dong, G.C., Zhao, Z.D., Hou, Z.Q., Zhou, S., Ke, S., 2008. Contribution of syncollisional felsic magmatism to continental crust growth: a case study of the Paleogene Linzizong volcanic succession in southern Tibet. *Chemical Geology* 250, 49-67.
- Morris, J., Leeman, W., Tera, F. (1990). The subducted component in island arc lavas: constraints from Be isotopes and B-Be systematics. *Nature* 344, 31-36.
- Nasdala, L., Wenzel, M., Vavra, G., Irmer, G., Wenzel, T., Kober, B., 2001. Metamictisation of natural zircon: accumulation versus thermal annealing of radioactivity-induced damage. *Contributions to mineralogy and petrology* 141, 125-144.
- Nichols, G. T., Wyllie, P. J., Stern, C. R. (1994). Subduction zone melting of pelagic sediments constrained by melting experiments. *Nature* 371, 785-788.
- Niu, Y.L., 2005. Generation and evolution of basaltic magmas: some basic concepts and a new view on the origin of Mesozoic–Cenozoic basaltic volcanism in eastern China. *Geological Journal of China Universities* 11, 9-46.
- Niu, Y., O'Hara, M.J., 2003. Origin of ocean island basalts: A new perspective from petrology, geochemistry, and mineral physics considerations. *Journal of Geophysical Research: Solid Earth* (1978–2012) 108.
- Niu, Y.L., O'Hara, M.J., 2009. MORB mantle hosts the missing Eu (Sr, Nb, Ta and Ti) in the continental crust: new perspectives on crustal growth, crust–mantle differentiation and

- chemical structure of oceanic upper mantle. *Lithos* 112, 1-17.
- Niu, Y.L., O'Hara, M.J., 2008. Global correlations of ocean ridge basalt chemistry with axial depth: a new perspective. *Journal of Petrology* 49, 633-664.
- Niu, Y.L., O'Hara, M.J., Pearce, J.A., 2003. Initiation of subduction zones as a consequence of lateral compositional buoyancy contrast within the lithosphere: a petrological perspective. *Journal of Petrology* 44, 851-866.
- Niu, Y.L., Zhao, Z.D., Zhu, D.C., Mo, X.X., 2013. Continental collision zones are primary sites for net continental crust growth-A testable hypothesis. *Earth-Science Reviews* 127, 96-110.
- Pearce, J.A., Harris, N.B., Tindle, A.G., 1984. Trace element discrimination diagrams for the tectonic interpretation of granitic rocks. *Journal of petrology* 25, 956-983.
- Pearce, J. A. & Peate, D. W. (1995). Tectonic implications of the composition of volcanic arc magmas. *Annual review of earth and planetary sciences* 23, 251-286.
- Pupin, J.P., 1980. Zircon and granite petrology. *Contributions to Mineralogy and Petrology* 73, 207-220.
- Qin, J.F., Lai, S.C., Grapes, R., Diwu, C.R., Ju, Y.J., Li, Y.F., 2009. Geochemical evidence for origin of magma mixing for the Triassic monzonitic granite and its enclaves at Mishuling in the Qinling orogen (central China). *Lithos* 112, 259-276.
- Qin, J.F., Lai, S.C., Li, Y.F., 2008a. Post-collisional plutonism with adakitic signatures: The Triassic Yangba granodiorite (Bikou terrane, northern Yangtze Block). *Chinese Journal of Geochemistry* 27, 72-81.
- Qin, J.F., Lai, S.C., Li, Y.F., 2008b. Slab breakoff model for the Triassic post-collisional adakitic granitoids in the Qinling Orogen, Central China: Zircon U-Pb ages, geochemistry, and

- Sr-Nd-Pb isotopic constraints. *International Geology Review* 50, 1080-1104.
- Ratschbacher, L., Hacker, B.R., Calvert, A., Webb, L.E., Grimmer, J.C., McWilliams, M.O., Ireland, T., Dong, S.W., Hu, J.M., 2003. Tectonics of the Qinling (Central China): tectonostratigraphy, geochronology, and deformation history. *Tectonophysics* 366, 1-53.
- Rudnick, R.L., Gao, S., 2003. Composition of the continental crust. *Treatise on geochemistry* 3, 1-64.
- Song, S.G., Niu, Y.L., Wei, C.J., Ji, J.Q., Su, L., 2010a. Metamorphism, anatexis, zircon ages and tectonic evolution of the Gongshan block in the northern Indochina continent-an eastern extension of the Lhasa Block. *Lithos* 120, 327-346.
- Song, S.G., Su, L., Li, X.H., Zhang, G.B., Niu, Y.L., Zhang, L.F., 2010b. Tracing the 850Ma continental flood basalts from a piece of subducted continental crust in the North Qaidam UHPM belt, NW China. *Precambrian Research* 183, 805-816.
- Sun, S.S., McDonough, W.F., 1989. Chemical and isotopic systematics of oceanic basalts: implications for mantle composition and processes. *Geological Society, London, Special Publications* 42, 313-345.
- Sun, W.D., Li, S.G., Chen, Y.D., Li, Y.J., 2002. Timing of Synorogenic Granitoids in the South Qinling, Central China: Constraints on the Evolution of the Qinling–Dabie Orogenic Belt. *The Journal of geology* 110, 457-468.
- Sun, W.D., Li, S.G., Zhang, H.F., Gao, S., Zhang, B.R., Luo, T.C., Ling, W.L., 1998. Pb isotopes of granitoids suggest Devonian accretion of the Yangtze (South China) craton to North China craton: comment and reply. *Geology* 29, 859-861.
- Vernon, R., 1984. Microgranitoid enclaves in granites-globules of hybrid magma quenched in a

plutonic environment.

- Vroon, P., Bergen, M. V., White, W., Varekamp, J. (1993). Sr–Nd–Pb isotope systematics of the Banda Arc, Indonesia: Combined subduction and assimilation of continental material. *Journal of Geophysical Research: Solid Earth* (1978–2012) 98, 22349–22366.
- Wang, X.X., Wang, T., Zhang, C.L., 2013. Neoproterozoic, Paleozoic, and Mesozoic granitoid magmatism in the Qinling Orogen, China: constraints on orogenic process. *Journal of Asian Earth Sciences* 72, 129–151.
- Wiedenbeck, M., Alle, P., Corfu, F., Griffin, W.L., Meier, M., Oberli, F., Quadt, A.V., Roddick, J.C., Spiegel, W., 1995. Three natural zircon standards for U–Th–Pb, Lu–Hf, trace element and REE analyses. *Geostandards newsletter* 19, 1–23.
- Xiao, Q.F., Qiu, R.Z., Deng, J.F., Li, T.D., Mo, X.X., Hong, D.W., Lu, X.X., Wang, T., Wu, F.Y., Xie, C.F., 2005. Granitoids and continental crustal growth modes in China. *Geology in China*, 32(3), 343–352 (in Chinese with English abstract).
- Xiao, Q.F., Deng, J., Qiu, R.Z., Liu, Y., Feng, Y.F., 2009. A preliminary study of the relationship between granitoids and the growth of continental crust: a case study of the formation of key orogen granitoids in China. *Geology in China*, 36(3): 594–622 (in Chinese with English abstract).
- Xu, J.F., Castillo, P.R., Li, X.H., Yu, X.Y., Zhang, B.R., Han, Y.W., 2002. MORB-type rocks from the Paleo-Tethyan Mian-Lueyang northern ophiolite in the Qinling Mountains, central China: implications for the source of the low $^{206}\text{Pb}/^{204}\text{Pb}$ and high $^{143}\text{Nd}/^{144}\text{Nd}$ mantle component in the Indian Ocean. *Earth and Planetary Science Letters* 198, 323–337.
- Xu, Y.L., Mao, Y.Z., Wang, G.G., 2006. Discuss on diagenetic and metallogenic features and

- metallogenic mechanism of Baijiazhaung Rock Mass in Minxian-Lixian area of Gansu Province. *Gansu geology*, 15(2): 36-41 (in Chinese with English abstract).
- Xue, F., Kröner, A., Reischmann, T., Lerch, F., 1996. Palaeozoic pre-and post-collision calc-alkaline magmatism in the Qinling orogenic belt, central China, as documented by zircon ages on granitoid rocks. *Journal of the Geological Society* 153, 409-417.
- Yang, L.Q., Deng, J., Qiu, K.F., Ji, X.Z., Santosh, M., Song, K.R., Song, Y.H., Geng, J.Z., Zhang, C., Hua, B., 2014. Magma mixing and crust-mantle interaction in the Triassic monzogranites of Bikou Terrane, central China: Constraints from petrology, geochemistry, and zircon U-Pb-Hf isotopic systematics. *Journal of Asian Earth Sciences*.
- Zhang, H.F., Jin, L.L., Zhang, L., Nigel, H., Zhou, L., Hu, S.H., Zhang, B.R., 2007. Geochemical and Pb-Sr-Nd isotopic compositions of granitoids from western Qinling belt: Constraints on basement nature and tectonic affinity. *Science in China Series D: Earth Sciences* 50, 184-196.
- Zhang, G.W., Cheng, S.Y., Guo, A.L., Dong, Y.P., Lai, S.C., Yao, A.P., 2004a. Mianlue paleo-suture on the southern margin of the Central Orogenic System in Qinling-Dabie with a discussion of the assembly of the mian part of the continent of China. *Geological Bulletin of China*, 846-853 (in Chinese with English abstract).
- Zhang, G.W., Guo, A.L., Yao, A.P., 2004b. Western Qinling – Songpan continental tectonic node in China's continental tectonics. *Earth Science Frontiers* (China University of Geosciences, Beijing), 23-32 (in Chinese with English abstract).
- Zhang, G.W., Liu, X.M., 1998. Some remarks on China Central Orogenic system. *Earth Science Frontiers* (China University of Geosciences, Beijing), 9-14 (in Chinese with English abstract).
- Zhang, R.Y., Liou, J.G., Ernst, W.G., 2009. The Dabie-Sulu continental collision zone: a

comprehensive review. *Gondwana Research* 16, 1-26.

Zhang, Z.Q., Zhang, G.W., Liu, D.Y., Wang, Z.Q., Tang, S.B., Wang, J.H., 2006. Isotopic Geochronology and Geochemistry of ophiolites, Granites and Clastic Sedimentary Rocks in the Qinling Orogenic Belt. Geological Publishing House, 1-348.

Zhu, X.Y., Chen, F.K., Li, S.Q., Yang, Y.Z., Nie, H., Siebel, W., Zhai, M.G., 2011. Crustal evolution of the North Qinling terrain of the Qinling Orogen, China: evidence from detrital zircon U–Pb ages and Hf isotopic composition. *Gondwana Research* 20, 194-204.

Figure Captions

Fig. 1. (a) Simplified geological framework of continental China (after Qin et al., 2009). (b) Simplified geological map showing the distribution of Triassic granitoids in the West Qinling Orogen (after Qin et al., 2009). (c) Geological map of the Baijiazhuang (BJZ) and Lvjing (LJ) plutons (after 1:250,000 geological map of Mianxian, Chinese Geological Survey, 2007).

Fig. 2. Photomicrographs of granitoid samples from the BJZ (a, b) and LJ (c, d) plutons. Field photos of MMEs in the host of the LJ pluton (e, f).

Fig. 3. LA-ICP-MS U-Pb concordia diagrams for zircons from the BJZ and LJ plutons.

Fig. 4. (a) TAS diagram and (b) A/NK [molar ratio $\text{Al}_2\text{O}_3/(\text{Na}_2\text{O} + \text{K}_2\text{O})$] vs. A/CNK [molar ratio $\text{Al}_2\text{O}_3/(\text{CaO} + \text{Na}_2\text{O} + \text{K}_2\text{O})$] of granitoids from the BJZ and LJ plutons.

Fig. 5. SiO_2 -variation diagrams of major element oxides of the BJZ and LJ plutons.

Fig. 6. Chondrite-normalized REE patterns (a, c) and primitive-mantle normalized trace element patterns (b, d) for granitoids of the BJZ and LJ plutons. Bulk continental crust (BCC) is from Rudnick and Gao (2003); chondrite and primitive mantle values are from Sun and McDonough (1989).

Fig. 7. (a) Initial ($^{87}\text{Sr}/^{86}\text{Sr}$) vs. $\epsilon_{\text{Nd}}(t)$ of granitoids of the BJZ and LJ plutons. For comparisons isotope compositions of the Guangtoushan-Miba pluton (Zhang et al., 2006), the Mishuling pluton (Qin et al., 2009) and the Wenquan pluton (Cao et al., 2011) in the West Qinling Orogen are also plotted. (b) Age vs. $\epsilon_{\text{Hf}}(t)$ of the BJZ and LJ plutons.

Fig. 8. Eu/Eu^* vs. Sr/Sr^* of granitoids from the BJZ and LJ plutons, $\text{Eu}/\text{Eu}^* =$

$2\text{Eu}_\text{N}/(\text{Sm}_\text{N}+\text{Gd}_\text{N})$, $\text{Sr}/\text{Sr}^* = 2\text{Sr}_\text{N}/(\text{Pr}_\text{N}+\text{Nd}_\text{N})$ following Niu and O'Hara (2009).

Fig. 9. Simple tectonic cartoon shows the formation of mantle-derived melt, partial melting of the lower continental crust and formation of widespread granitoids in the West Qinling Orogen.

Fig. 1

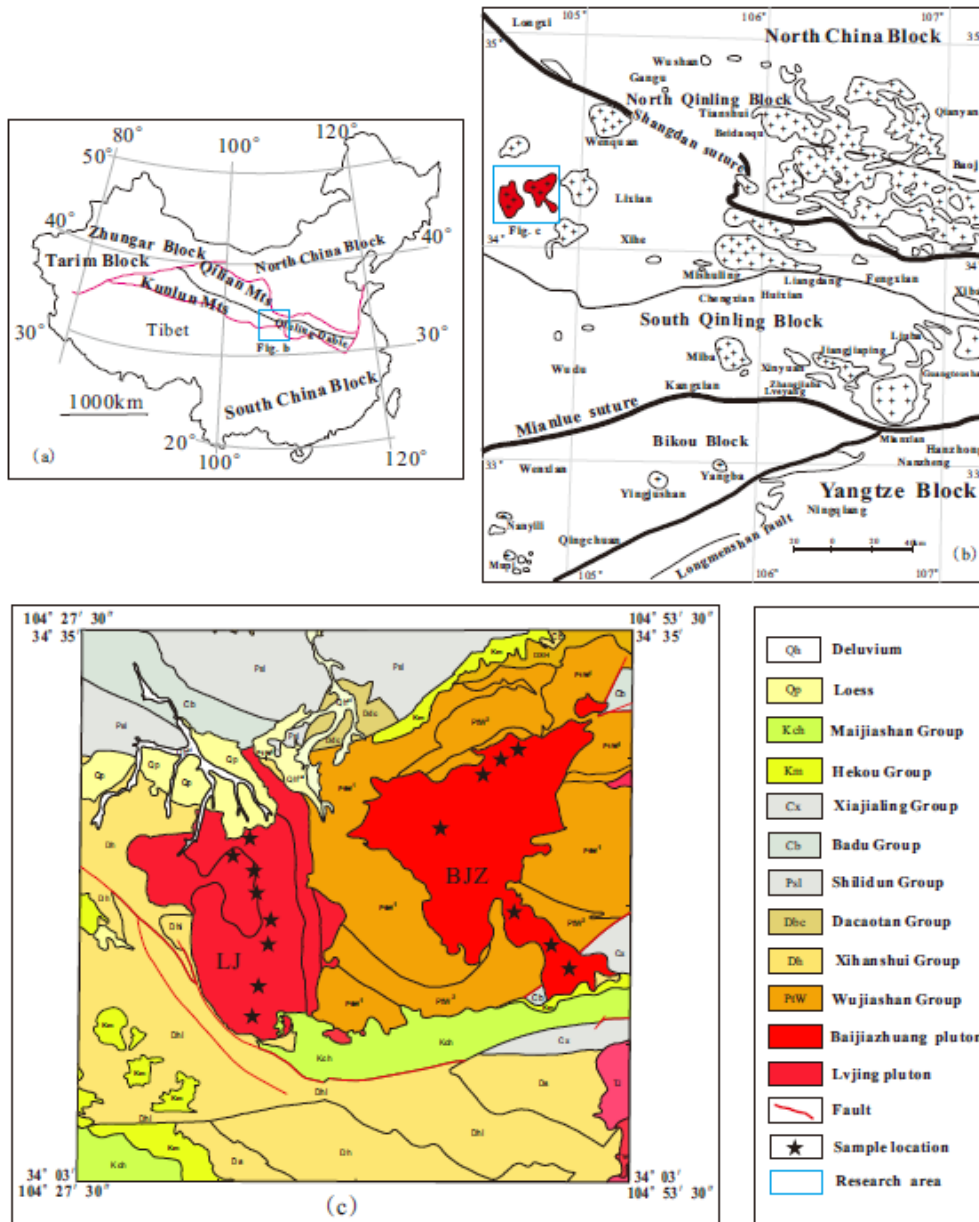


Fig. 2

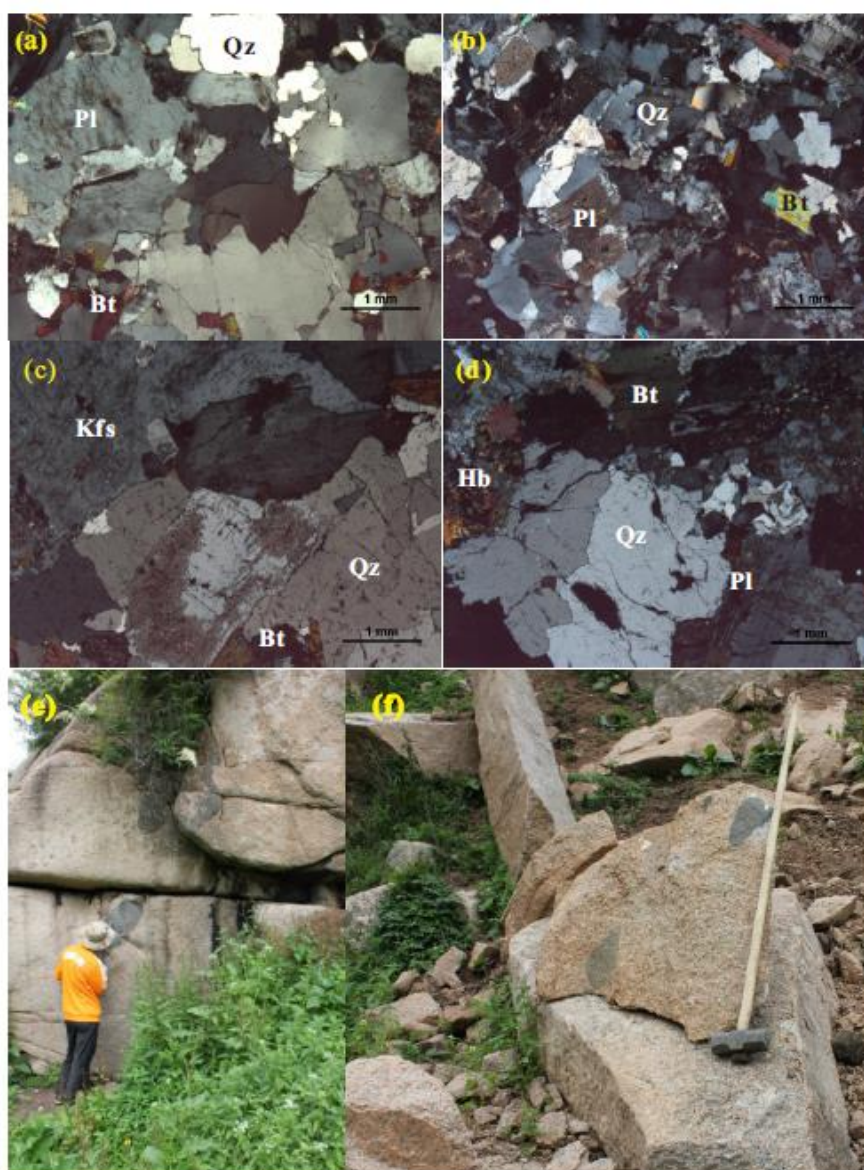


Fig. 3

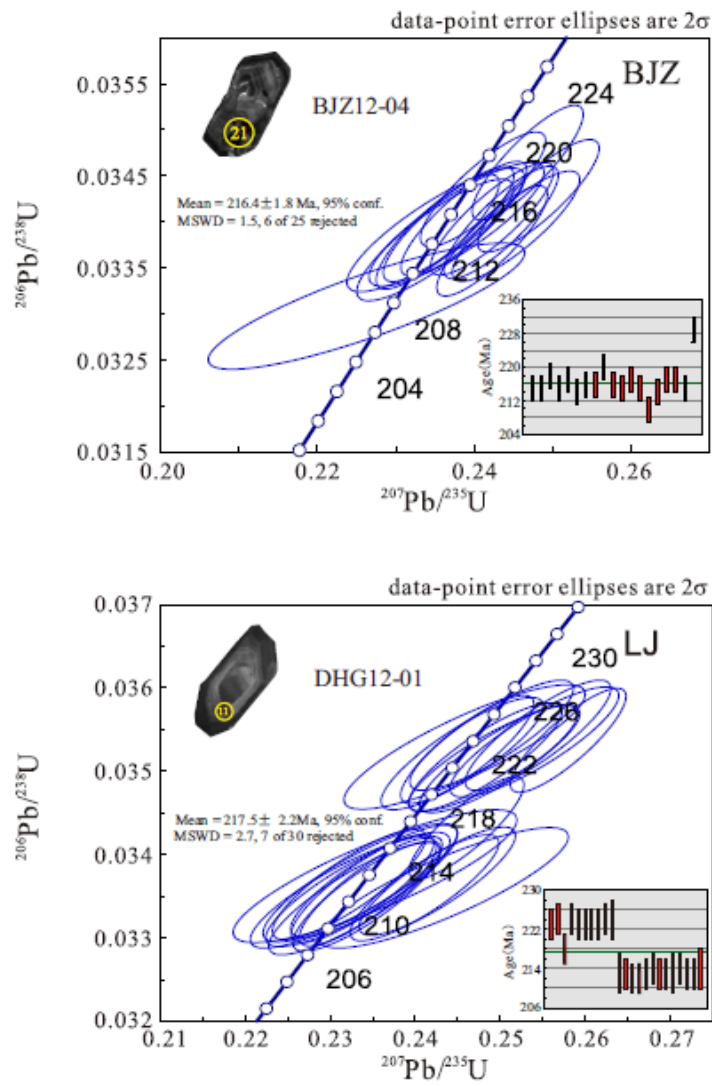


Fig. 4

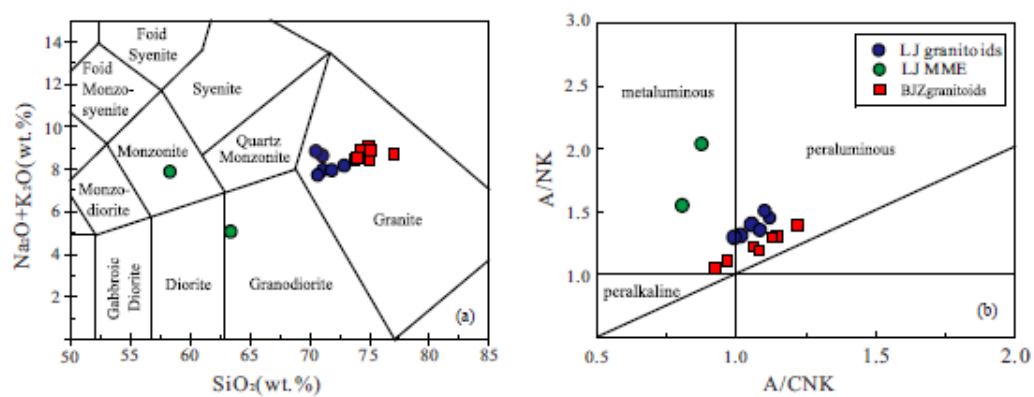


Fig. 5

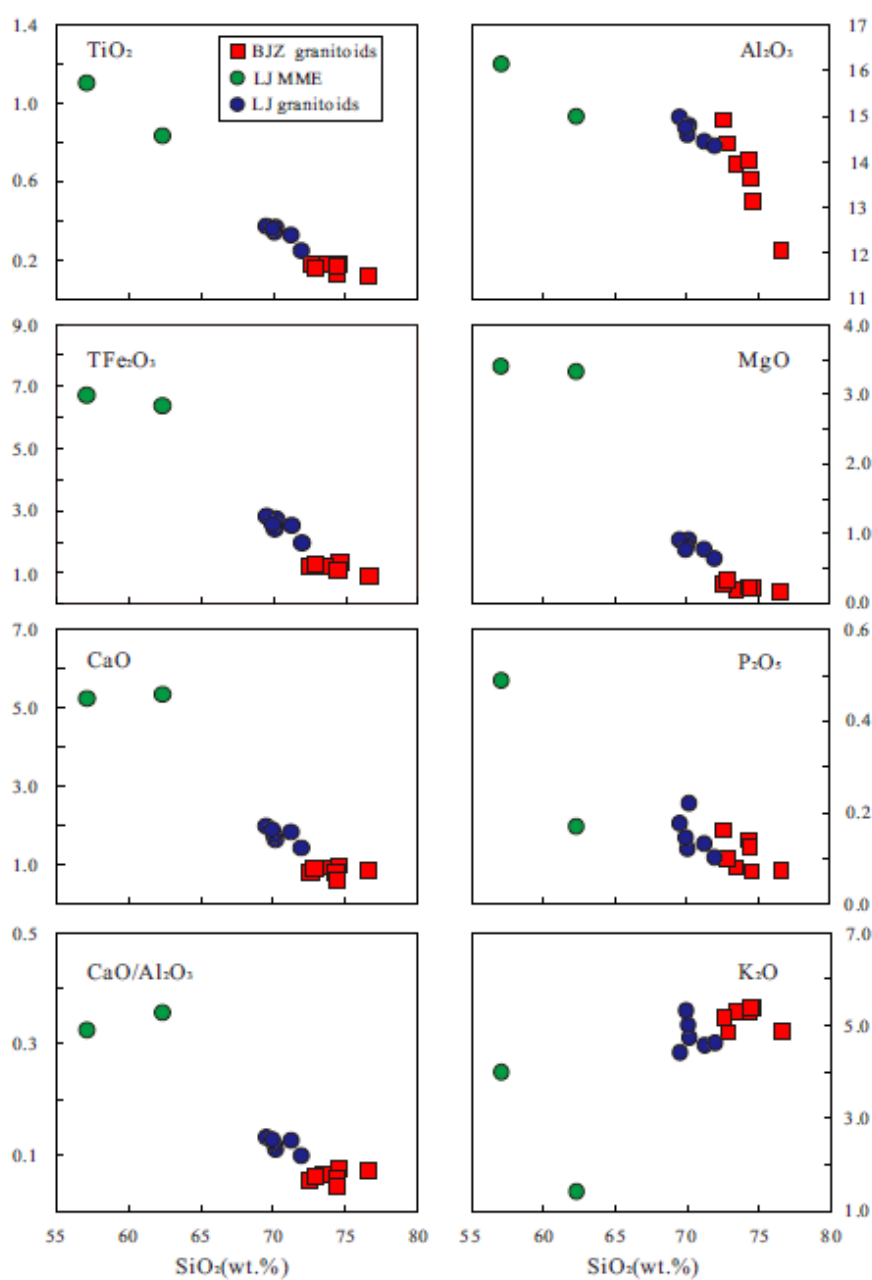


Fig. 6

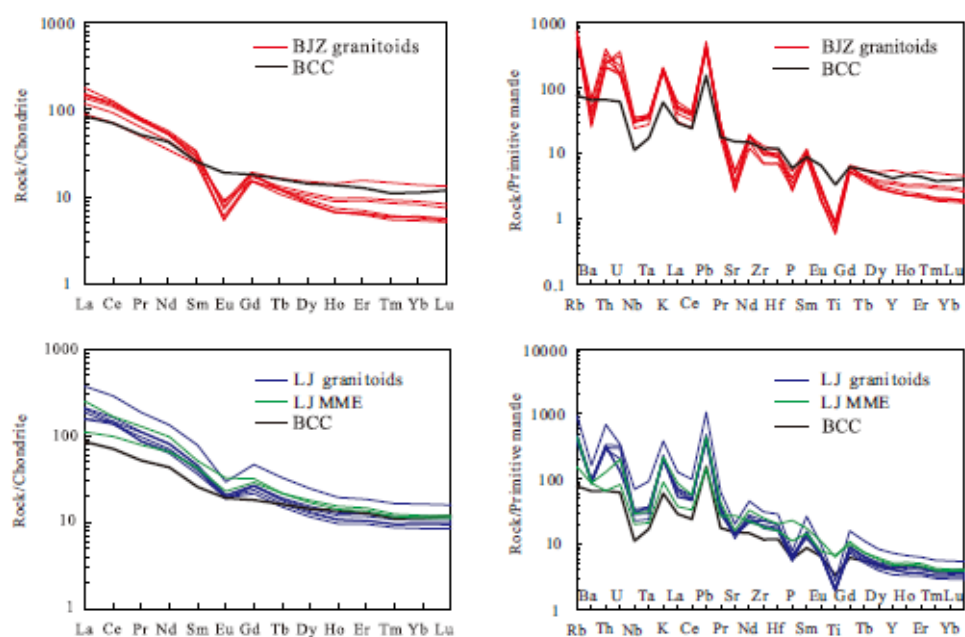


Fig. 7

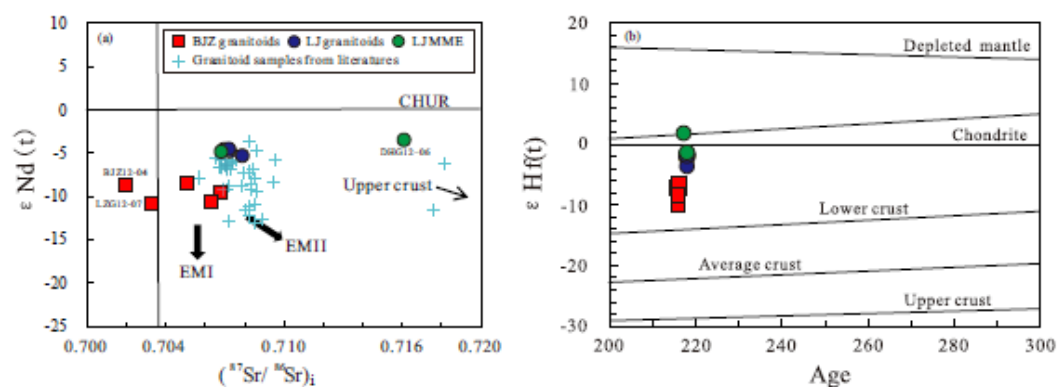


Fig. 8

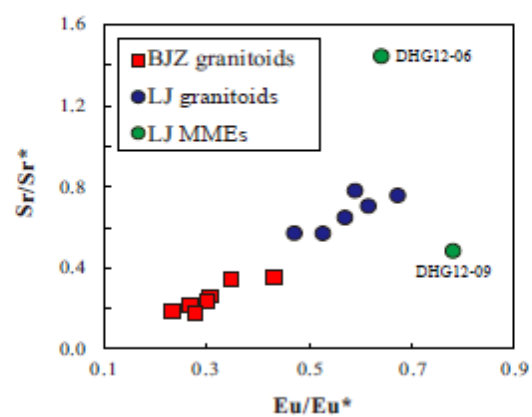
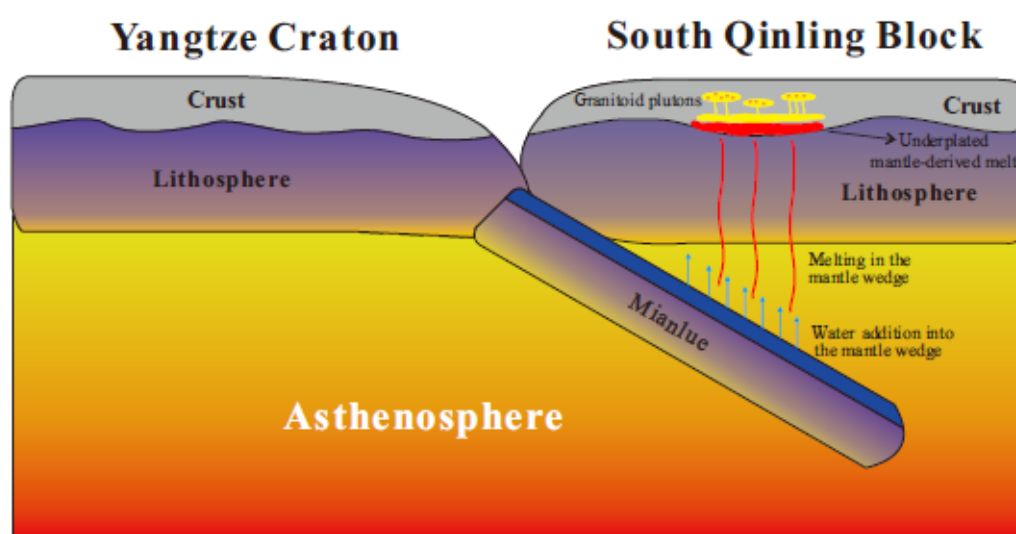
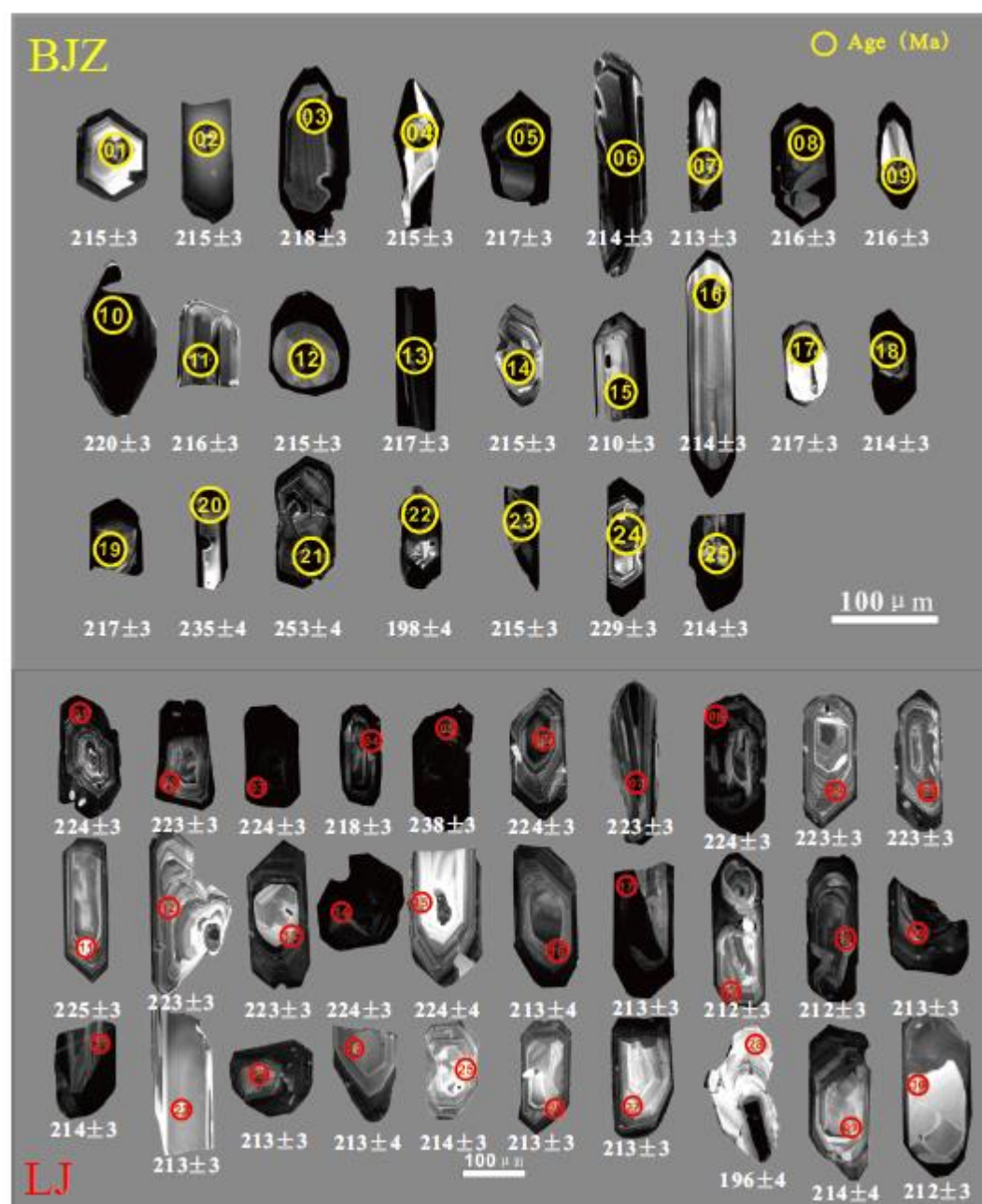


Fig. 9



Appendix 1



Cathodoluminescence (CL) images of representative zircons from the host granitoids of the BJZ and LJ plutons. Spots for zircon U-Pb dating using LA-ICP-MS and ages derived from zircons are also shown.

Appendix 2. U-Th-Pb SHRIMP zircon data of granitoids and MME from Baijiazhuang(BJZ) and Lvjing(LJ) pluton

Spot	Content (ppm)				Ratios								Age(Ma)								Discordance
	Th	U	Pb	Th/U	$^{207}\text{Pb}/^{206}\text{Pb}$		$^{207}\text{Pb}/^{235}\text{U}$		$^{206}\text{Pb}/^{238}\text{U}$		$^{208}\text{Pb}/^{232}\text{Th}$		$^{207}\text{Pb}/^{206}\text{Pb}$		$^{207}\text{Pb}/^{235}\text{U}$		$^{206}\text{Pb}/^{238}\text{U}$		$^{208}\text{Pb}/^{232}\text{Th}$		
					b	1σ	U	1σ	U	1σ	h	1σ	b	1σ	U	σ	U	σ	h	σ	
BJ4-01	404.		50.9	0.28		0.001		0.006		0.000		0.000									
	9	1441	0	1	0.0519	2	0.2434	0	0.0340	5	0.0099	3	282	30	221	5	215	3	200	5	2.79%
BJ4-02	140.	786.	27.0	0.17		0.001		0.006		0.000		0.000									
	6	9	5	9	0.0505	4	0.2367	8	0.0340	5	0.0100	4	219	39	216	6	215	3	200	8	0.47%
BJ4-03	92.9	943.	32.1	0.09		0.001		0.006		0.000		0.000									
	9	8	6	9	0.0509	3	0.2411	5	0.0344	5	0.0102	5	237	36	219	5	218	3	205	9	0.46%
BJ4-04	254.	410.	15.7	0.61		0.002		0.009		0.000		0.000									
	2	5	3	9	0.0503	0	0.2351	3	0.0339	6	0.0105	3	207	61	214	8	215	3	212	6	-0.47%
BJ4-05	205.		37.8	0.18		0.001		0.006		0.000		0.000									
	0	1084	6	9	0.0525	3	0.2482	3	0.0343	5	0.0110	3	307	32	225	5	217	3	220	6	3.69%
BJ4-06	399.		51.4	0.27		0.001		0.005		0.000		0.000									
	9	1473	0	2	0.0520	2	0.2423	8	0.0338	5	0.0099	2	285	29	220	5	214	3	199	5	2.80%
BJ4-07	640.	982.	39.5	0.65		0.001		0.008		0.000		0.000		12							
	5	2	3	2	0.0721	7	0.3393	4	0.0341	5	0.0121	3	584	2	247	11	213	3	209	3	15.96%
BJ4-08	196.	806.	28.3	0.24		0.001		0.006		0.000		0.000									
	5	7	1	4	0.0509	4	0.2387	6	0.0340	5	0.0112	3	234	37	217	5	216	3	225	6	0.46%
BJ4-09	263.	720.	26.0	0.36		0.001		0.007		0.000		0.000									
	8	3	9	6	0.0536	5	0.2520	2	0.0341	5	0.0106	3	353	37	228	6	216	3	214	6	5.56%
BJ4-10	118.		87.2	0.04		0.001		0.005		0.000		0.000									
	6	2582	0	6	0.0517	2	0.2468	8	0.0346	5	0.0108	4	271	28	224	5	220	3	216	8	1.82%
BJ4-11	281.	1069	38.2	0.26	0.0516	0.001	0.2423	0.006	0.0340	0.000	0.0134	0.000	269	35	220	5	216	3	268	6	1.85%

	7	0	4		3	4	5	3													
BJ4-12	267.	373.	14.6	0.71		0.001	0.009	0.000	0.000												
	8	5	1	7	0.0508	9	0.2377	1	0.0340	6	0.0107	3	229	59	217	7	215	3	215	6	0.93%
BJ4-13	572.		48.5	0.43		0.001	0.006	0.000	0.000												
	2	1316	9	5	0.0535	3	0.2520	3	0.0342	5	0.0109	3	349	31	228	5	217	3	219	5	5.07%
BJ4-14	311.		49.2	0.21		0.001	0.006	0.000	0.000												
	0	1430	2	8	0.0504	3	0.2353	4	0.0339	5	0.0103	3	211	36	215	5	215	3	207	6	0.00%
BJ4-15	371.	416.	16.9	0.89		0.002	0.009	0.000	0.000					17							
	1	5	9	1	0.0580	1	0.2673	8	0.0334	5	0.0113	3	176	0	207	14	210	3	210	3	-1.43%
BJ4-16	220.	500.	18.1	0.44		0.001	0.008	0.000	0.000												
	2	5	7	0	0.0504	7	0.2350	2	0.0338	5	0.0105	3	214	51	214	7	214	3	211	6	0.00%
BJ4-17	282.	477.	18.2	0.59		0.001	0.008	0.000	0.000												
	7	1	5	3	0.0535	8	0.2532	5	0.0343	5	0.0106	3	351	48	229	7	217	3	213	6	5.53%
BJ4-18	688.		116.	0.22		0.001	0.009	0.000	0.000												
	9	3137	3	0	0.0829	9	0.3939	3	0.0344	5	0.0163	4	889	79	282	8	214	3	207	3	31.78%
BJ4-19	547.		75.2	0.25		0.001	0.006	0.000	0.000												
	4	2135	6	6	0.0547	2	0.2579	1	0.0342	5	0.0109	3	398	28	233	5	217	3	220	5	7.37%
BJ4-20	863.		112.	0.33		0.002	0.014	0.000	0.000					10							
	2	2599	7	2	0.0966	6	0.5100	0	0.0383	6	0.0181	5	1061	0	329	13	235	4	225	4	40.00%
BJ4-21	905.		129.	0.34		0.002	0.014	0.000	0.000					11							
	0	2658	4	1	0.0995	5	0.5756	6	0.0419	7	0.0233	6	808	8	316	14	253	4	246	4	24.90%
BJ4-22			81.2	1.06		0.004	0.025	0.000	0.000					27							
	1436	1342	8	9	0.2040	8	1.0534	6	0.0374	6	0.0215	5	1112	0	289	32	198	4	188	3	45.96%
BJ4-23	269.		74.4	0.12		0.001	0.006	0.000	0.000												
	3	2206	7	2	0.0535	2	0.2508	1	0.0340	5	0.0115	3	303	72	223	5	215	3	214	3	3.72%

BJ4-24	197.		138.	0.05		0.001		0.008		0.000		0.000											
	7	3729	9	3	0.0682	6	0.3462	5	0.0368	6	0.0340	9	448	78	250	7	229	3	227	6	9.17%		
BJ4-25	638.		68.4	0.41		0.002		0.014		0.000		0.000		14									
	2	1526	5	8	0.1179	7	0.5895	3	0.0362	5	0.0226	5	773	6	268	15	214	3	208	4	25.23%		
DH1-0	432.	960.	36.0	0.45		0.001		0.005		0.000		0.000											
	1	8	2	4	1	0.0529	1	0.2580	6	0.0354	5	0.0097	2	324	25	233	4	224	3	195	4	4.02%	
DH1-0	429.		44.7	0.35		0.001		0.005		0.000		0.000											
	2	7	1200	3	8	0.0535	0	0.2597	3	0.0352	5	0.0116	2	260	85	226	7	223	3	222	3	1.35%	
DH1-0	164.	367.	14.0	0.44		0.001		0.007		0.000		0.000											
	3	1	8	7	6	0.0521	4	0.2545	0	0.0354	5	0.0116	3	288	36	230	6	224	3	233	5	2.68%	
DH1-0	336.	939.	34.1	0.35		0.001		0.005		0.000		0.000											
	4	0	2	2	8	0.0520	1	0.2460	5	0.0343	5	0.0115	2	285	26	223	5	218	3	231	5	2.29%	
DH1-0	432.		56.7	0.30		0.001		0.006		0.000		0.000											
	5	6	1412	2	6	0.0609	1	0.3185	1	0.0379	5	0.0137	3	405	78	254	7	238	3	236	3	6.72%	
DH1-0	219.	367.	14.5	0.59		0.001		0.008		0.000		0.000											
	6	1	1	8	7	0.0521	6	0.2540	1	0.0354	5	0.0118	3	290	45	230	7	224	3	237	5	2.68%	
DH1-0	267.	395.	15.8	0.67		0.001		0.007		0.000		0.000											
	7	7	2	5	7	0.0515	5	0.2498	6	0.0352	5	0.0114	2	265	43	226	6	223	3	230	5	1.35%	
DH1-0	431.		51.9	0.30		0.001		0.005		0.000		0.000											
	8	2	1405	6	7	0.0555	0	0.2702	5	0.0353	5	0.0114	2	430	22	243	4	224	3	230	4	8.48%	
DH1-0	253.	514.	19.8	0.49		0.001		0.007		0.000		0.000											
	9	3	2	3	3	0.0545	5	0.2643	3	0.0352	5	0.0115	3	390	35	238	6	223	3	232	5	6.73%	
DH1-1	210.	470.	17.9	0.44		0.001		0.007		0.000		0.000											
	0	8	3	4	8	0.0512	5	0.2483	4	0.0352	5	0.0118	3	249	41	225	6	223	3	237	5	0.90%	
DH1-1	343.	453.	18.8	0.75	0.0552	0.001	0.2700	0.007	0.0355	0.000	0.0119	0.000	421	35	243	6	225	3	240	5	8.00%		

DH1-2	191.	201.	8.42	0.95		0.002		0.009		0.000		0.000										
4	7	4	0	2	0.0503	0	0.2335	3	0.0337	6	0.0094	3	209	61	213	8	213	4	189	5	0.00%	
DH1-2	144.	365.	13.3	0.39		0.001		0.007		0.000		0.000										
5	7	8	8	6	0.0522	6	0.2426	5	0.0337	5	0.0093	3	295	43	221	6	214	3	188	5	3.27%	
DH1-2	128.	519.	18.2	0.24		0.001		0.006		0.000		0.000										
6	4	3	1	7	0.0507	4	0.2344	6	0.0336	5	0.0096	3	225	37	214	5	213	3	193	6	0.47%	
DH1-2	108.	221.	8.23	0.49		0.001		0.008		0.000		0.000										
7	4	0	9	1	0.0504	9	0.2333	9	0.0336	6	0.0092	3	212	57	213	7	213	3	185	6	0.00%	
DH1-2	80.5	167.	7.90	0.48		0.004		0.020		0.000		0.000		23								
8	0	4	4	1	0.1355	5	0.6357	7	0.0340	6	0.0233	7	692	4	239	22	196	4	190	4	21.94%	
DH1-2	80.6	143.	5.38	0.56		0.003		0.013		0.000		0.000										
9	2	0	2	4	0.0506	0	0.2353	7	0.0337	7	0.0084	4	221	98	215	11	214	4	168	8	0.47%	
DH1-3	285.	422.	16.9	0.67		0.002		0.009		0.000		0.000										
0	5	7	4	5	0.0615	1	0.2841	8	0.0335	6	0.0103	3	657	46	254	8	212	3	207	6	19.81%	

Appendix 3. Major elements (wt.%) and trace elements (ppm) compositions of granitoids samples from Baijiazhuang and Lvjing pluton

Pluton	Lvjing								Baijiazhuang							
Rock type	granitoids								granitoids							
Sample	DHG 12-03	DHG 12-10	DHG 12-17	DHG 12-18	DHG 12-20	DHG 12-24	DHG 12-06	DHG 12-09	BJZ1 2-03	BJZ1 2-04	BJZ1 2-05	LZG 12-02	LZG 12-03	LZG 12-05	LZG 12-07	
SiO ₂	70.17	70.07	71.24	69.52	71.95	69.94	62.31	57.07	74.58	76.60	73.47	74.37	72.58	72.86	74.44	
TiO ₂	0.37	0.34	0.33	0.37	0.25	0.36	0.83	1.10	0.17	0.12	0.17	0.12	0.18	0.15	0.17	
Al ₂ O ₃	14.80	14.59	14.45	14.99	14.35	14.76	15.00	16.14	13.15	12.07	13.96	14.04	14.91	14.41	13.63	
TFE ₂ O ₃	2.73	2.41	2.52	2.82	1.96	2.57	6.37	6.71	1.30	0.88	1.19	1.06	1.19	1.28	1.08	
MnO	0.06	0.05	0.06	0.06	0.05	0.06	0.13	0.18	0.05	0.05	0.05	0.02	0.03	0.05	0.05	
MgO	0.91	0.82	0.77	0.91	0.64	0.77	3.32	3.40	0.22	0.16	0.20	0.23	0.27	0.33	0.22	
CaO	1.64	1.76	1.84	1.99	1.43	1.90	5.34	5.24	0.98	0.87	0.93	0.82	0.81	0.91	0.62	
Na ₂ O	3.08	3.48	3.27	3.14	3.40	3.43	3.54	3.71	3.63	3.75	3.46	3.07	3.12	3.56	3.42	
K ₂ O	4.74	5.01	4.57	4.41	4.62	5.32	1.42	3.99	5.38	4.89	5.30	5.28	5.17	4.85	5.39	
P ₂ O ₅	0.22	0.12	0.13	0.18	0.10	0.15	0.17	0.49	0.07	0.07	0.08	0.14	0.16	0.10	0.12	
LOI	0.93	0.62	0.65	0.74	0.63	0.6	0.98	1.17	0.47	0.61	0.59	0.78	0.94	0.79	0.87	
Total	99.64	99.28	99.83	99.13	99.38	99.83	99.42	99.20	100.00	100.07	99.40	99.95	99.36	99.29	100.02	
Li	68.52	75.76	100.6	52.80	230.2	71.50	29.10	103.4	121.1	130.5	119.7	104.1	71.80	106.7	70.68	
Sc	5.456	4.904	5.268	5.566	8.208	5.004	33.68	15.34	1.729	1.871	0.878	2.135	2.56	1.846	1.174	
V	39.84	36.46	33.66	38.98	44.04	38.06	203.8	161.4	12.28	4.400	3.700	3.856	5.522	7.874	3.868	
Cr	15.66	13.33	11.92	14.84	16.00	13.04	37.88	16.47	3.070	2.652	2.942	6.086	3.156	11.02	2.632	
Co	4.586	4.350	3.918	4.802	5.204	4.650	24.40	19.63	1.014	0.459	0.402	0.471	0.578	0.968	0.548	
Ni	6.384	4.742	3.892	5.794	6.106	5.372	20.58	10.20	0.941	0.923	2.008	1.889	1.364	7.716	0.794	
Cu	2.778	2.448	3.174	2.976	5.940	2.400	8.560	131.2	2.714	1.086	0.966	2.010	2.336	3.856	1.040	
Zn	60.20	60.90	63.18	55.22	97.08	42.92	91.84	91.28	71.68	61.94	84.06	57.66	61.90	57.80	76.64	

Ga	20.92	21.02	22.48	21.04	45.02	19.24	29.18	20.18	22.60	23.30	20.52	20.69	22.90	22.66	23.46
Rb	290.2	278.0	283.0	254.6	575.4	231.6	96.70	279.4	425.8	424.6	460.6	349.3	363.0	368.4	457.4
Sr	298.4	289.2	257.8	304.6	431.2	289.8	579.8	341.6	105.6	55.98	56.00	58.47	77.44	114.3	61.98
Y	21.68	18.09	18.73	20.26	33.18	15.49	23.24	21.72	25.14	15.53	16.86	13.18	11.49	11.70	11.84
Zr	256.0	210.6	194.4	257.6	350.2	219.2	203.2	281.6	144.3	78.86	^{105.8} ₄	77.31	114.8	124.5	110.6
Nb	22.67	20.59	24.38	21.84	49.60	16.31	14.34	21.02	24.40	22.45	25.20	17.30	21.18	21.84	21.90
Cs	11.56	12.88	24.90	12.35	31.68	9.098	5.930	14.14	17.18	24.96	22.38	21.51	13.07	16.90	9.828
Ba	684.2	635.6	593.4	647.2	1130	638.6	599.2	611.2	458.6	176.3	196.5	240.4	320.8	453.0	271.0
Ba															
La	36.54	43.50	47.86	49.34	87.40	36.90	26.00	58.82	36.36	27.80	32.26	21.07	34.82	42.30	34.62
Ce	82.96	83.14	88.62	98.66	174.8	88.72	59.76	100.9	70.24	56.52	66.50	43.42	75.34	77.30	70.62
Pr	8.242	9.132	10.32	10.54	17.57	8.090	7.394	12.06	7.284	6.038	7.088	4.732	7.368	7.538	7.678
Nd	30.90	32.66	36.90	37.82	61.80	29.08	30.32	45.10	24.72	20.58	24.38	16.24	25.18	24.46	26.66
Sm	6.438	6.002	6.792	6.954	11.87	5.470	6.448	7.792	4.592	3.928	4.508	3.690	4.980	4.102	5.174
Eu	1.163	1.118	1.073	1.191	1.688	1.112	1.315	1.868	0.495	0.317	0.313	0.350	0.446	0.527	0.420
Gd	5.336	4.812	5.330	5.498	9.512	4.388	5.908	6.510	3.936	3.080	3.510	3.143	3.778	3.138	3.746
Tb	0.711	0.610	0.664	0.692	1.217	0.560	0.803	0.804	0.610	0.452	0.494	0.459	0.464	0.404	0.449
Dy	3.858	3.186	3.370	3.650	6.202	2.922	4.522	4.262	3.800	2.622	2.816	2.388	2.230	2.108	2.164
Ho	0.719	0.597	0.608	0.672	1.091	0.541	0.862	0.792	0.803	0.500	0.543	0.416	0.378	0.375	0.374
Er	2.078	1.731	1.708	1.929	3.034	1.572	2.414	2.236	2.546	1.494	1.602	1.149	1.030	1.068	1.059
Tm	0.297	0.244	0.239	0.274	0.418	0.220	0.314	0.294	0.370	0.215	0.234	0.155	0.138	0.149	0.149
Yb	1.980	1.653	1.595	1.798	2.742	1.435	2.024	1.910	2.332	1.386	1.510	0.972	0.902	0.987	1.012
Lu	0.294	0.246	0.238	0.268	0.400	0.214	0.299	0.284	0.337	0.190	0.210	0.133	0.129	0.143	0.142
Hf	6.159	5.115	4.957	6.134	8.947	5.525	4.940	6.288	3.444	2.142	2.692	2.183	3.026	2.972	2.816
Ta	1.483	1.201	1.524	1.404	3.776	0.991	0.873	1.297	1.612	1.467	1.522	1.130	1.466	1.355	1.486
Pb	31.02	31.64	34.12	29.32	74.46	26.62	10.41	31.08	27.76	29.52	31.34	36.31	32.34	25.92	31.48
Th	26.02	25.48	27.88	28.58	57.76	24.14	5.596	10.84	23.58	17.54	20.26	17.75	27.48	33.54	20.32
U	2.822	6.158	2.692	6.836	7.122	4.292	1.727	4.200	3.588	3.342	7.516	3.575	4.588	3.408	6.468

Appendix 4. Whole-rock Sr-Nd-Hf isotopic composition for granitoids and MME from Baijiazhuang and Lvjing pluton

Pluton	Rock type	Sample	Rb (ppm)	Sr (ppm)	$^{87}\text{Rb}/^{86}\text{Sr}$	$^{87}\text{Sr}/^{86}\text{Sr}$	$(^{87}\text{Sr}/^{86}\text{Sr})_i$	Sm (ppm)	Nd (ppm)	$^{147}\text{Sm}/^{144}\text{Nd}$	$^{143}\text{Nd}/^{144}\text{Nd}$	2σ	$(^{143}\text{Nd}/^{144}\text{Nd})_i$	ϵNd (t)	T_{DM} (Ma)	Lu (ppm)	Hf (ppm)	$^{176}\text{Lu}/^{177}\text{Hf}$	$^{176}\text{Hf}/^{177}\text{Hf}$	2σ	$(^{176}\text{Hf}/^{177}\text{Hf})_i$	ϵHf (t)	T_{DM1} (Ma)	T_{DM2} (Ma)
	MME	DHG1 2-06	96.7	579.8	0.483	0.717633	0.7161	6.448	30.32	0.129	0.512361	0.000008	0.5122	-3.52	1425	0.299	4.94	0.009	0.282739	0.000005	0.2827	2.41	911	1160
		DHG1 2-09	279.4	341.6	2.367	0.714237	0.7068	7.792	45.1	0.105	0.512255	0.000007	0.5121	-4.90	1256	0.284	6.288	0.006	0.282624	0.000006	0.2826	-1.34	1039	1419
LJ	granitoids	DHG1 2-10	278	289.2	2.782	0.715673	0.7070	6.002	32.66	0.112	0.512279	0.000009	0.5121	-4.62	1302	0.246	5.115	0.007	0.282602	0.000004	0.2826	-2.18	1089	1468
		DHG1 2-18	254.6	304.6	2.419	0.71484	0.7073	6.954	37.82	0.112	0.512269	0.000011	0.5121	-4.82	1318	0.268	6.134	0.006	0.282607	0.000005	0.2826	-1.91	1060	1457
		DHG1 2-20	575.4	431.2	3.862	0.720001	0.7079	11.87	61.8	0.117	0.512249	0.000007	0.5121	-5.35	1417	0.4	8.947	0.006	0.282560	0.000006	0.2825	-3.59	1142	1563
		DHG1 2-24	231.6	289.8	2.313	0.714468	0.7072	5.47	29.08	0.114	0.512286	0.000011	0.5121	-4.56	1326	0.214	5.525	0.005	0.282609	0.000005	0.2826	-1.74	1034	1453
BJZ	granitoids	BJZ12-03	425.8	105.6	11.67	0.741559	0.7050	4.592	24.72	0.113	0.512082	0.000010	0.5119	-8.50	1614	0.337	3.444	0.014	0.282457	0.000005	0.2824	-8.33	1705	1788
		BJZ12-04	424.6	55.98	21.95	0.770614	0.7019	3.928	20.58	0.116	0.512071	0.000008	0.5119	-8.80	1682	0.19	2.142	0.013	0.282485	0.000004	0.2824	-7.15	1565	1727
		LZG12-02	349.3	58.47	17.29	0.760931	0.7068	3.69	16.24	0.138	0.512060	0.000008	0.5119	-9.64	2194	0.133	2.183	0.009	0.282492	0.000003	0.2825	-6.33	1348	1714
		LZG12-05	368.4	114.3	9.328	0.735462	0.7063	4.102	24.46	0.102	0.511954	0.000009	0.5118	-10.69	1629	0.143	2.972	0.007	0.282377	0.000005	0.2823	-10.14	1462	1971
		LZG12	457.4	61.9	21.36	0.770	0.7033	5.147	26.66	0.118	0.511963	0.000	0.5118	-10.	1875	0.142	2.816	0.007	0.2824	0.000	0.2824	-8.3	1390	1855

-07 8 092 010 95 29 004 5

$$\begin{aligned}
 (^{87}\text{Sr}/^{86}\text{Sr})_i &= (^{87}\text{Sr}/^{86}\text{Sr})_{\text{Sample}} - ^{87}\text{Rb}/^{86}\text{Sr}(e^{\lambda t} - 1), \lambda = 1.42 \times 10^{-11} \text{a}^{-1}, t = 220 \text{ Ma}. \\
 (^{143}\text{Nd}/^{144}\text{Nd})_i &= (^{143}\text{Nd}/^{144}\text{Nd}) - (^{147}\text{Sm}/^{144}\text{Nd}) \times (e^{\lambda t} - 1), \varepsilon_{\text{Nd}}(t) = [(^{143}\text{Nd}/^{144}\text{Nd}) / (^{143}\text{Nd}/^{144}\text{Nd})_{\text{CHUR}}(t) - 1] \times 10^4, \\
 (^{143}\text{Nd}/^{144}\text{Nd})_{\text{CHUR}}(t) &= 0.512638 - 0.1967 \times (e^{\lambda t} - 1), T_{\text{DM}} = 1/\lambda \times \ln\{1 + [((^{143}\text{Nd}/^{144}\text{Nd}) - 0.51315) / ((^{147}\text{Sm}/^{144}\text{Nd}) - 0.21317)]\}, \lambda_{\text{Sm-Nd}} = 6.54 \times 10^{-12} \text{a}^{-1}. \\
 (^{176}\text{Hf}/^{177}\text{Hf})_i &= [(^{176}\text{Hf}/^{177}\text{Hf}) - (^{176}\text{Lu}/^{177}\text{Hf}) \times (e^{\lambda t} - 1)], \varepsilon_{\text{Hf}}(t) = [(^{176}\text{Hf}/^{177}\text{Hf}) / (^{176}\text{Hf}/^{177}\text{Hf})_{\text{CHUR}}(t) - 1] \times 10^4, T_{\text{DM1}} = 1/\lambda \times \ln[1 + ((^{176}\text{Hf}/^{177}\text{Hf})_{\text{Sample}} - \\
 (^{176}\text{Hf}/^{177}\text{Hf})_{\text{DM}}) / ((^{176}\text{Lu}/^{177}\text{Hf})_{\text{Sample}} - (^{176}\text{Lu}/^{177}\text{Hf})_{\text{DM}})], T_{\text{DM2}} &= T_{\text{DM1}} - (T_{\text{DM1}} - t)((f_{\text{CC}} - f_{\text{Sample}}) / (f_{\text{CC}} - f_{\text{DM}})), f_{\text{Lu-Hf}} = (^{176}\text{Lu}/^{177}\text{Hf})_{\text{Sample}} / (^{176}\text{Lu}/^{177}\text{Hf})_{\text{CHUR}} - 1, \\
 (^{176}\text{Lu}/^{177}\text{Hf})_{\text{CHUR}} &= 0.0332, (^{176}\text{Hf}/^{177}\text{Hf})_{\text{CHUR},0} = 0.282785, (^{176}\text{Lu}/^{177}\text{Hf})_{\text{DM}} = 0.0384, (^{176}\text{Hf}/^{177}\text{Hf})_{\text{DM}} = 0.28325, f_{\text{CC}}, f_{\text{Sample}}, f_{\text{DM}} \text{ are their own } f_{\text{Lu-Hf}}, \lambda = 1.867 \times 10^{-11} \text{a}^{-1}.
 \end{aligned}$$

Highlights:

1. Our granitoids originate from partial melting of the lower continental crust
2. Isotope compositions of the granitoids indicate mantle-crust interaction
3. Mantle-derived melt was from partial melting of the mantle wedge
4. Water from the subducted oceanic slab caused partial melting of the mantle wedge